MID-AMERICA TRANSPORTATION CENTER

Report # MATC-KU: 151-1

Final Report
WBS: 25-1121-0005-151-1

Automated Bridge Inspection using Digital Image Correlation Phase I: Methodology Development

William Collins, PhD, PE
Assistant Professor
CEAE Department
University of Kansas

Caroline Bennett, PhD, PE
Professor

Jian Li, PhD, PE
Associate Professor

Elaina J. Sutley, PhD
Assitant Professor

Mary Juno
Research Assistant

Hayder Al-Salih
Research Assistant

Landon Dellenbaugh
Research Assistant

2020

A Cooperative Research Project sponsored by
U.S. Department of Transportation- Office of the Assistant Secretary for Research and Technology

MATC

Automated Bridge Inspection using Digital Image Correlation Phase I: Methodology Development

William Collins, Ph.D., P.E.
Assistant Professor
CEAE Department
University of Kansas

Caroline Bennett, Ph.D., P.E.
Professor
CEAE Department
University of Kansas

Jian Li, Ph.D., P.E.
Associate Professor
CEAE Department
University of Kansas

Elaina J. Sutley, Ph.D.
Assistant Professor
CEAE Department
University of Kansas

Mary Juno
Research Assistant
CEAE Department
University of Kansas

Hayder Al-Salih
Research Assistant
CEAE Department
University of Kansas

Landon Dellenbaugh
Research Assistant
CEAE Department
University of Kansas

A Report on Research Sponsored by

Mid-America Transportation Center

University of Nebraska–Lincoln

December 2019

TECHNICAL REPORT DOCUMENTATION PAGE

1. Report No. 25-1121-0005-151-1	2. Government Accession No.	3. Recipient's Catalog No.
4. Title and Subtitle Automated Bridge Inspection using Digital Image Correlation Phase I: Methodology Development		5. Report Date January 2020 6. Performing Organization Code
7. Author(s) Collins, William N. ORCID: 0000-0002-2835-6389 Bennett, Caroline R. ORCID: 0000-0002-2713-0011 Li, Jian ORCID: 0000-0003-3439-7539 Sutley, Elaina J. ORCID: 0000-0002-4749-2538 Dellenbaugh, Landon; Al-Salih, Hayder; and Juno, Mary.		8. Performing Organization Report No. 25-1121-0005-151-1
9. Performing Organization Name and Address University of Kansas 2150 Learned Hall 1530 W. 15th St. Lawrence, KS 66049		10. Work Unit No. 11. Contract or Grant No. 69A3551747107
12. Sponsoring Agency Name and Address Mid-America Transportation Center 2200 Vine St PO Box 830851 Lincoln, NE 68583-0851		13. Type of Report and Period Covered Final Report (December 2017-December 2018) 14. Sponsoring Agency Code MATC TRB RiP No. 91994-6

15. Supplementary Notes
Conducted in cooperation with the U.S. Department of Transportation, Federal Highway Administration.

16. Abstract

Distortion-induced fatigue cracks are a major concern in steel bridges built prior to the 1980s in the United States. Distortion-induced fatigue cracks make up the majority of fatigue cracks in bridges, but Departments of Transportation have to primarily rely on the use of visual inspections to locate and characterize fatigue cracking, despite recent studies proving that visual inspections fail to consistently identify realistically sized fatigue cracks. Many fatigue crack detection methodologies have been proposed and examined, but the methods are dependent on detection equipment physically attached to the bridge, such as sensor networks. This limits the effectiveness and flexibility of the methods for sensing multiple fatigue susceptible regions. Developing an inspection technique that does not rely on human visual inspection or physical attachments has the potential to reduce the risk of injury to inspectors, increase reliability, and decrease the time and cost of performing inspections.

Vision-based technologies are an active are of research working to develop alternatives to manual inspections of transportation infrastructure. While many vision-based technologies focus on macro-indicators of damage, digital image correlation (DIC) has shown promise for detecting and characterizing fatigue cracks. DIC measurements have the ability to capture full-field displacements and surface strains, allowing for the potential of identifying and characterizing both in-plane and out-of-plane fatigue cracks, such as those occurring on steel bridges exposed to loading through differential girder displacement. This paper describes an experimental study in which a methodology for crack detection was formulated using an in-plane test specimen and then tested on a scaled steel girder-to-cross frame specimen to evaluate the success of the method at detecting out-of-plane cracking. Preliminary results indicate that DIC is successful at locating cracks and determining the length of the crack.

17. Key Words	18. Distribution Statement
Fatigue, cracking, bridge, steel, inspection, digital image correlation	

19. Security Classif. (of this report)	20. Security Classif. (of this page)	21. No. of Pages	22. Price
		81	

Form DOT F 1700.7 (8-72) Reproduction of completed page authorized

Table of Contents

List of Figures

List of Tables

Disclaimer

The contents of this report reflect the views of the authors, who are responsible for the facts and the accuracy of the information presented herein. This document is disseminated in the interest of information exchange. The report is funded, partially or entirely, by a grant from the U.S. Department of Transportation's University Transportation Centers Program. However, the U.S. Government assumes no liability for the contents or use thereof.

Abstract

Distortion-induced fatigue cracks are a major concern in steel bridges built prior to the 1980s in the United States. Distortion-induced fatigue cracks make up the majority of fatigue cracks in bridges, but Departments of Transportation have to primarily rely on the use of visual inspections to locate and characterize fatigue cracking, despite recent studies proving that visual inspections fail to consistently identify realistically sized fatigue cracks. Many fatigue crack detection methodologies have been proposed and examined, but the methods are dependent on detection equipment physically attached to the bridge, such as sensor networks. This limits the effectiveness and flexibility of the methods for sensing multiple fatigue susceptible regions. Developing an inspection technique that does not rely on human visual inspection or physical attachments has the potential to reduce the risk of injury to inspectors, increase reliability, and decrease the time and cost of performing inspections.

Vision-based technologies are an active arc of research working to develop alternatives to manual inspections of transportation infrastructure. While many vision-based technologies focus on macro-indicators of damage, digital image correlation (DIC) has shown promise for detecting and characterizing fatigue cracks. DIC measurements have the ability to capture full-field displacements and surface strains, allowing for the potential of identifying and characterizing both in-plane and out-of-plane fatigue cracks, such as those occurring on steel bridges exposed to loading through differential girder displacement. This paper describes an experimental study in which a methodology for crack detection was formulated using an in-plane test specimen and then tested on a scaled steel girder-to-cross frame specimen to evaluate the success of the method at detecting out-of-plane cracking. Preliminary results indicate that DIC is successful at locating cracks and determining the length of the crack.

Chapter 1 Digital Image Correlation Background

1.1 Introduction

Bridges are vital for the movement of people and goods across the country, but due to their long service life and the repetitive loads they are subjected to, they are prone to damage or deterioration. Recently, the American Society of Civil Engineers gave bridges in the United States a grade of C+, while over 9 percent of the bridges are considered to be structurally deficient (ASCE 2017). Properly maintaining bridges and identifying and correcting potential issues is vital in ensuring that they remain in-service for the entirety of their intended service life or longer.

One of the main concerns for aging steel bridges is the initiation and propagation of fatigue cracks (Fisher 1984). Fatigue cracks are caused by cyclic traffic loading and are initially very small and challenging to detect through visual inspection. Undetected cracks have the potential to propagate to a critical size, which could compromise the structural integrity of the bridge. A primary concern is distortion-induced fatigue cracks, which account for almost 90% of fatigue cracks in aging steel bridges in the United States (Connor and Fisher 2006). Older steel bridges were regularly designed without a connection between the flanges and connection plate. When such a bridge experiences loading from traffic, it undergoes differential deflection between the girders. The differential deflection allows the cross frame to push or pull on the girder web, causing out-of-plane stresses to be applied to the weak web gap region, resulting in distortion-induced fatigue. Distortion-induced fatigue cracks are common in steel bridges built prior to the 1980s in the United States due to the time's design practices (Zhao and Roddis 2004). To minimize the impact of distortion-induced fatigue, aging bridges have required regular inspection, as well as repairs and protective measures such as retrofitting.

Bridge inspections are typically performed on a 24-month cycle (FHWA 2004), and the most common method for detecting fatigue cracks is a visual inspection. This presents challenges since fatigue cracks are initially small, and therefore difficult to detect using visual inspection. When cracks go undetected, however, they can propagate to sizes that have the potential to compromise a bridge's structural integrity. Despite the importance of inspections to ensure the safety of bridge infrastructure, visual inspections have significant monetary and time costs, as well as presenting safety risks to both the inspectors and the traveling public. Additionally, consistently identifying realistic fatigue cracks successfully has been proven to be extremely difficult (Whitehead 2015; Zhao and Haldar 1996).

Researchers in both the structural health monitoring and non-destructive testing communities have evaluated technologies to detect and monitor cracks. Sensing technologies have been used to detect and monitor cracking, both for in- and out-of-plane fatigue loading, but many of these approaches require the use sensors or other components that were physically attached to the bridge, preventing these methodologies from effectively monitoring the various fatigue susceptible regions on steel bridges. A computer vision-based detection technology would operate without dependence on a physical attachment, allowing large sections of steel bridges to be surveyed efficiently and safely.

There has been some research on vision-based crack detection methodologies, but testing has primarily been conducted under highly idealized conditions, such as in-plane fatigue loading, or has focused on non-metallic materials. Minimal research with vision-based crack detection methods has been conducted on out-of-plane loading or with the complex geometries found on steel highway bridges. Utilizing digital image correlation, vision-based crack detection

performance is being tested, on both idealized, in-plane lab setups and out-of-plane test setups with complex geometry.

1.2 Fatigue and Fracture Mechanics

Fatigue cracking has the potential to pose serious risks to the structural integrity of either single components or entire systems. Fatigue cracking most commonly occurs in steel components that are subject to cyclic loading. While cyclic loading is typically below the ultimate strength of the steel, repeated loading can lead to system failure. Fatigue cracks can be caused by cyclic loading, and the risk of fatigue cracks is increased in materials with stress raiser. Stress raisers are typically discontinuities in the material, such as holes, grooves, fillets, and scratches. These can cause a concentration of stress in a single location, which can allow fatigue cracks to initiate where the stress is highest. Increased stresses caused by stress raisers can be quantified using a stress concentration factor, in a process known as the Stress-Based Approach, if the material is still in the linear-elastic range.

Stress concentration factors are based on the geometry of the discontinuity. For a circular hole, the stress concentration factor is three. As the circle becomes more elliptical, or infinitely sharp, like a crack, the Stress-Based Approach methodology is of little use as the crack tip stress concentration theoretically approaches infinity. Other approaches are the Strain-Based Approach, which looks at localized yielding during cyclic loading, and the Fracture Mechanics Approach, which considers both linear-elastic and elastic-plastic behavior. The Fracture Mechanics Approach defines a stress intensity factor, K, characterizing the stress state at the crack tip, and is the primary method used in this study to define behavior.

There are three modes of fatigue crack propagation. Mode I is the crack opening mode, Mode II is in-plane shearing or the “sliding” mode, and Mode III is the anti-plane shearing or the

"tearing" mode. Mode I and III are the focus of this report with In-Plane loading referring to Mode I loading, and Out-of-Plane referring primarily to Mode III loading.

1.3 Digital Image Correlation Methodology

1.3.1 Computer Vision

Computer vision is the branch of technology that uses computer algorithms and optics to gather information from pictures and videos. Various uses for computer vision have been evaluated for engineering and material science applications, particularly to characterize mechanical parameters. The potential of using computer vision for crack detection has been evaluated by many researchers, using a variety of materials. For example, edge detection methodologies have been used to successfully find edge-like features on digital images, leading to detection and localization of cracks in concrete surfaces (Abdel-Qader et al. 2003). Edge detection in metallic materials has a high rate of false positives resulting from inadvertent detection of surface textures, component boundaries, defects, and corrosion (Yeum and Dyke 2015).

Some research has been conducted to develop algorithms to remove short, thick, or exceedingly linear edges that are typically not created by cracking, with the goal of creating a reliable crack detection method (Yu et al. 2007). Other researchers have created complex algorithms to detect cracking in asphalt and concrete pavements (Yamaguchi and Hashimoto 2010; Zou et al. 2012; Cha et al. 2017). Typically, these materials have larger crack openings, as well as higher contrast between cracked and uncracked regions compared to metallic materials, meaning that applying the edge detection methodologies to steel bridges is challenging. Additionally, the majority of computer vision studies focus on macro-indicators of damage, such

as extensive corrosion, concrete deck deterioration, and large displacements caused by substructure movement.

1.3.2 Digital Image Correlation Background

Digital image correlation (DIC) is a subset of computer vision that uses medium- to high-resolution cameras and post-processing computer software to analyze images resulting in full-field surface displacement. A three-dimensional strain field can then be developed using the displacement. DIC software can analyze both two- and three- dimensional data, depending on the number of cameras utilized during testing. DIC operates by comparing a series of images collected during loading and generates relative displacement and strain for each point on the image. DIC has shown potential for detecting and characterizing fatigue cracks, but most testing has been limited to simplified setups, either utilizing in-plane loading or simple geometry.

DIC has been used in material testing to determine both strain and deformation and can be used instead of traditional sensing methods, like strain gauges or extensometers (Yuan et al. 2014). Evaluating cracking using DIC has been applied in detecting cracks in a concrete structure (Küntz et al. 2006) and in stress intensity factors calculations (Zhang and He 2012). Previous researchers have evaluated limitations of 3D DIC using simplified test setups, and applications of 3D DIC has been explored since the mid-1990s (Helm et al. 1996). Four camera setups have been used to determine out-of-plane displacements, but the additional cameras result in challenges with the experimental setup and calibration. (Chen et al. 2013). A stereoscopic camera setup with a high shutter speed has been used to measure full-field out-of-plane vibrations, but the high-speed cameras result in a lack of image resolution (Helfrick et al. 2010). Complex loading scenarios have been tested using clevis fixtures to create mixed-mode loading of compact tension (C(T)) specimens. For the opening (Mode I) and in-plane shear (Mode II)

loading, displacement results using DIC agreed with results developed from finite element analysis of the crack (Sutton et al. 2007).

Extensive research has been performed on the applications of DIC to identify fatigue cracks in metallic materials in idealized laboratory settings. Studies have previously examined in-plane fatigue cracking, with the goal of identifying and characterizing the crack. In-plane loading studies have been performed on steel C(T) specimens (Rupil et al. 2011), aluminum channels (Vanlanduit et al. 2008), notched tension specimens (Carrol et al. 2009; Carrol et al. 2012), and tension plates with center drilled bolt holes (Lorenzino et al. 2014; Hutt and Cawley 2009). These studies have helped to show the limitations and abilities of DIC in detecting cracks. Most of these studies, however, involved qualitative crack identification and characterization. The development of a quantifiable methodology for automated bridge inspections has only been minimally investigated. Additionally, out-of-plane loading conditions have not been researched as thoroughly as in-plane fatigue loading. The minimal experimental evaluation of out-of-plane fatigue loading is possibly due to the sophistication and complexity required for the test setups (Sutton et al. 2007).

1.3.3 Digital Image Correlation Setup

In order to ensure accurate results from the DIC software, the preparation of the specimen, camera setup, calibration, and image collection all need to be optimized. The preparation of the specimen primarily involves applying a speckle pattern. The ideal pattern is high contrast and random, with consistent dot sizes. The speckle pattern creates points of reference for comparison of the images. Without a speckle pattern, there are no reference points for evaluating the movement of the specimen. Choosing the correct camera setup depends on the test specimen's complexity. For two-dimensional analysis, one camera will suffice, since no out-

of-plane deformations are expected. This allows for a simplified test setup, as well as an easier calibration. When testing for out-of-plane displacements, two or more cameras are needed to ensure that the strain field is three-dimensional. Calibration of the cameras converts the images from pixels to the real dimensions and ensures that the image can be evaluated realistically. After calibration, while the test is running, images are collected at a constant interval during loading. These images are then analyzed using the DIC software to determine full-field displacements.

Chapter 2 In-Plane Testing

2.1 In-Plane C(T) Test Setup and Loading

2.1.1 Test Setup

Initial testing was performed to develop quantifiable crack length methodologies that could be applied to complex out-of-plane geometries. Testing was initially performed on a compact tension (C(T)) specimen loaded in a servo-hydraulic testing machine. The C(T) specimen was loaded cyclically, and fatigue cracks were initiated and propagated to certain test lengths. The C(T) specimen used was 6.35 mm (0.25 in.) thick, with a width of 127 mm (5.0 in.), allowing for long crack lengths to form. Fatigue and fracture mechanics typically measures the crack length from the load line, which includes a portion of the machined notch. When using DIC to characterize fatigue cracks, measuring the crack from the tip of the notch is more appropriate, as shown in Figure 2.1.

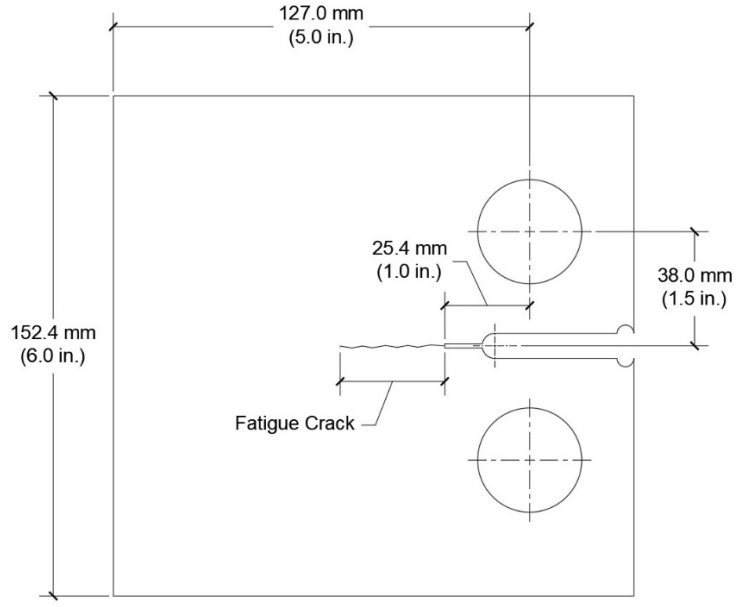

Figure 2.1 In-plane specimen dimensions

2.1.2 Test Loading Protocol

Because of the differing loading that highway bridges can be subjected to; any fatigue crack inspection methodology needs to be able to operate over a range of load magnitudes. Five loading cases were defined using the stress intensity ranges of 11, 22, 33, 44, and 55 MPa√m (10, 20, 30, 40, and 50 ksi√in) and were designated as LC1 through LC5, as indicated in table 2.1. The ratio of minimum to maximum load, the R-ratio, for all load cases was 0.1. Each load case was evaluated for four different crack lengths, from 12.7 to 50.8 mm (0.5 to 2.0 in.) in 12.7 mm (0.5 in.) increments. To limit excessive crack tip plasticity, crack propagation was conducted at low stress levels, and the lowest stress intensity was tested first and increased to the highest. Additionally, once testing concluded for each crack length, the crack was grown at a low stress intensity range, ensuring that the crack extended beyond any previously induced plastic zone.

Table 2.1 In-plane loading cases

Load Case	**Stress Intensity Factor MPa√m (ksi√in)**
LC1	11 (10)
LC2	22 (20)
LC3	33 (30)
LC4	44 (40)
LC5	55 (50)

2.1.3 DIC Configuration

During the testing of the C(T) specimen, the DIC testing was performed with a single camera. No out-of-plane displacement was expected, allowing one camera, with a 17 mm (0.67 in.) lens, to evaluate the displacement occurring. The camera was mounted onto a tripod, and a

single, external LED light was used to minimize shadows and provide increased contrast between the specimen and the speckle pattern.

2.2 Crack Characterization Methodology

Methodologies for interpreting DIC data, whether displacement or calculated strain, vary between researchers, but often require visual identification of the crack by the operator. Although crack location can be easily identified whether using strain or displacement, as seen in Figure 2.2, automating crack detection requires the development or use of algorithms that function without operator interaction.

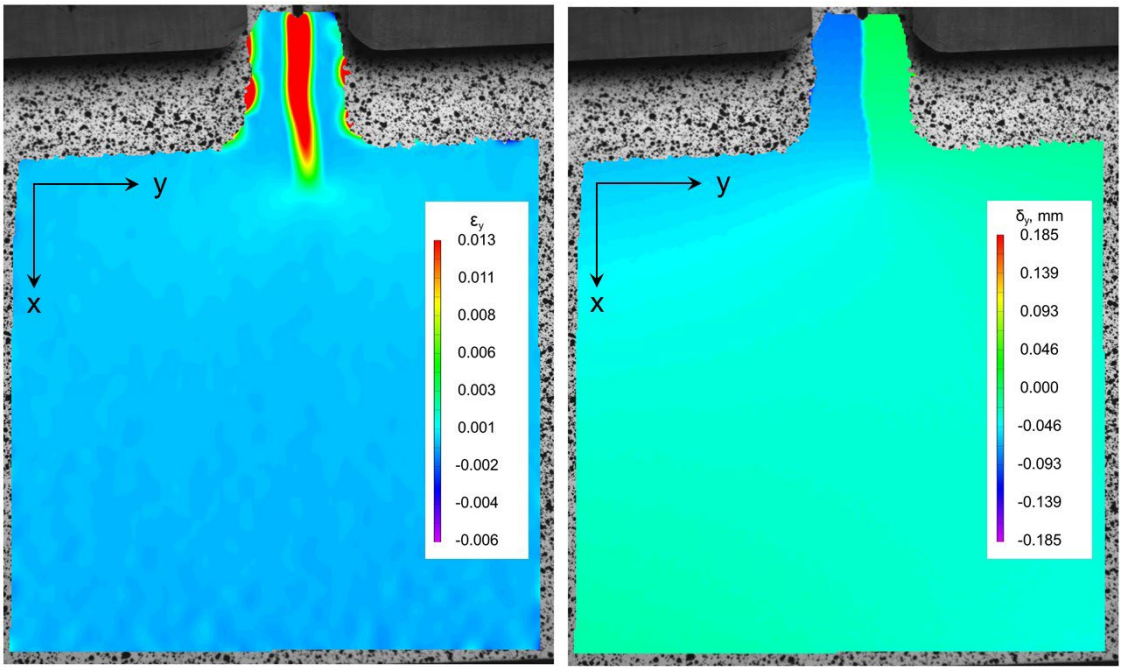

Figure 2.2 Typical DIC results showing crack location for in-plane testing in terms of a) strain and b) displacement

The images collected were primarily analyzed using coordinate transformation. Initially the y-axis had to be aligned to the load line, while the x-axis was aligned to the crack path. The

crack location was easily identifiable visually, but the end goal of automation prompted the development of algorithms to determine crack length from the collected DIC data. Initial analysis was performed by imputing the full-field y-axis displacement contours into MATLAB as a matrix. Despite the false positives often produced by edge detection algorithms when attempting to locate fatigue cracks on steel bridges, edge detection works well for DIC images. A simple edge detection algorithm was utilized to evaluate the contour data, allowing for the localization of the crack path along specific x-y coordinates. Once the exact crack location was determined, evenly spaced, orthogonal lines, represented by the dashed lines, were drawn along the crack path, represented schematically as the bi-linear line (fig. 2.3a). The displacement along each orthogonal line was used to determine relative displacement, defined as the difference between plateau values on either side of the crack (fig. 2.3b). For each orthogonal line, the relative displacement can be plotted along the length of the crack, similar to that shown in Figure 2.3c.

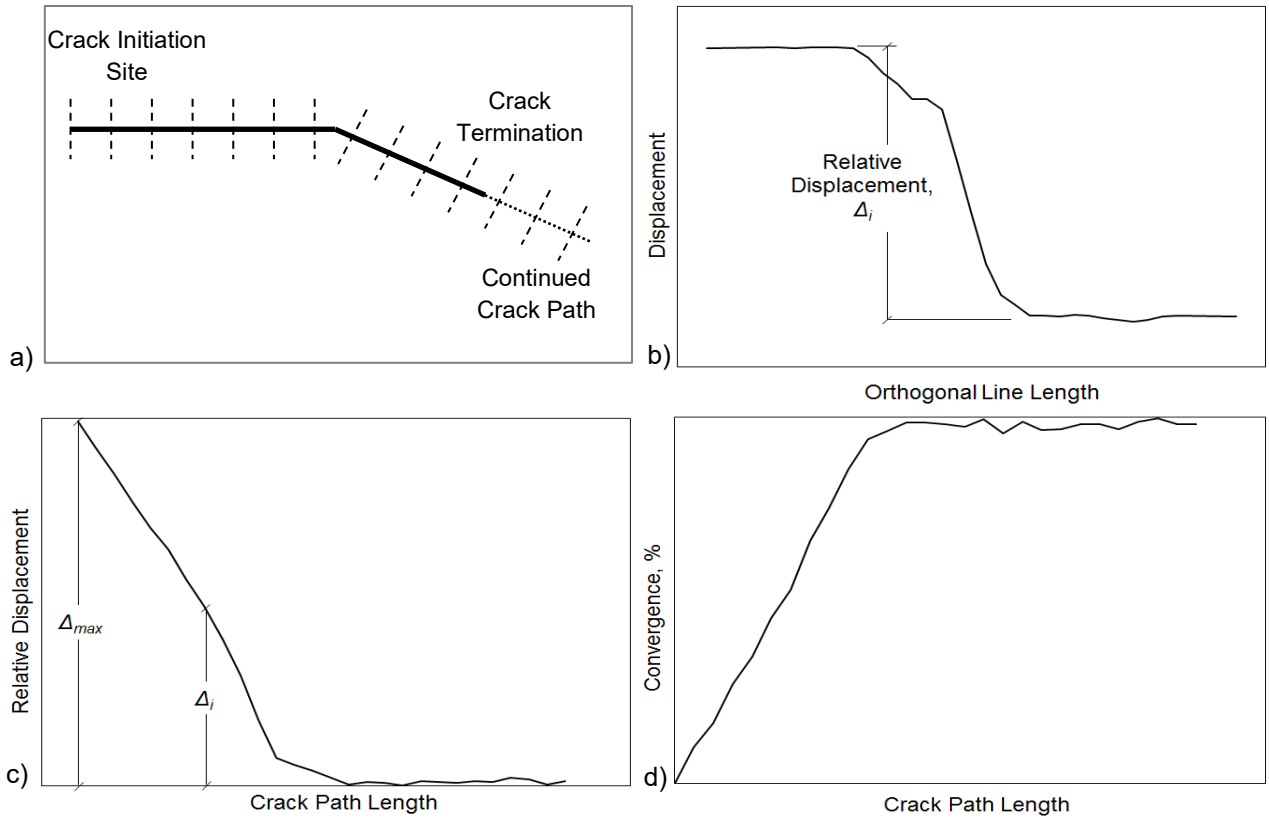

Figure 2.3 a) Crack path and data export lines, b) Displacement values along a data export line, c) Relative displacement along crack path, and d) Convergence along crack path

The convergence of relative displacement along the crack path, shown in fig. 2-3d, was calculated using

$$\text{Convergence } = 100\% - \frac{\Delta_i}{\Delta_{max}} \tag{2.1}$$

where Δ_i is the relative displacement along the crack path and Δ_{max} is the maximum relative displacement along the crack length, which typically occurred at the crack initiation site. As the crack opening approaches zero at the crack tip, the convergence of relative displacement theoretically approaches 100%.

2.3 In-Plane Testing Results

The crack characterization methodology described was performed for each load case at each crack length. Convergence values theoretically should approach 100% as the crack tip is approached, but results indicate that this not what actually occurs, likely due to the resolution of the collected images. The convergence plot for the 25.4 mm (1.0 in.) crack length is shown in Figure 2.4. The dotted vertical line represents the crack length measured through specimen compliance and optically verified. The convergence plots for all in-plane crack lengths, as well as the raw and DIC-analyzed figures, can been found in Appendix A. For each in-plane specimen trial, the convergence values at known crack lengths were determined for all load cases, shown in table 2.2. For crack lengths of 25.4, 38.1, and 50.8 mm (1.0, 1.5, 2.0 in.) most load cases had convergence values of over 90%, with many over 95%. The convergence values for the 12.7 mm (0.5 in.) crack did not perform as well. This was likely because of localized behavior due to the proximity to the machined notch. As loading was increased during testing, the convergence values tended to decrease, indicating that relative displacement continued beyond the crack tip. This might have been caused by crack tip plasticity, which was induced at higher applied stress intensities.

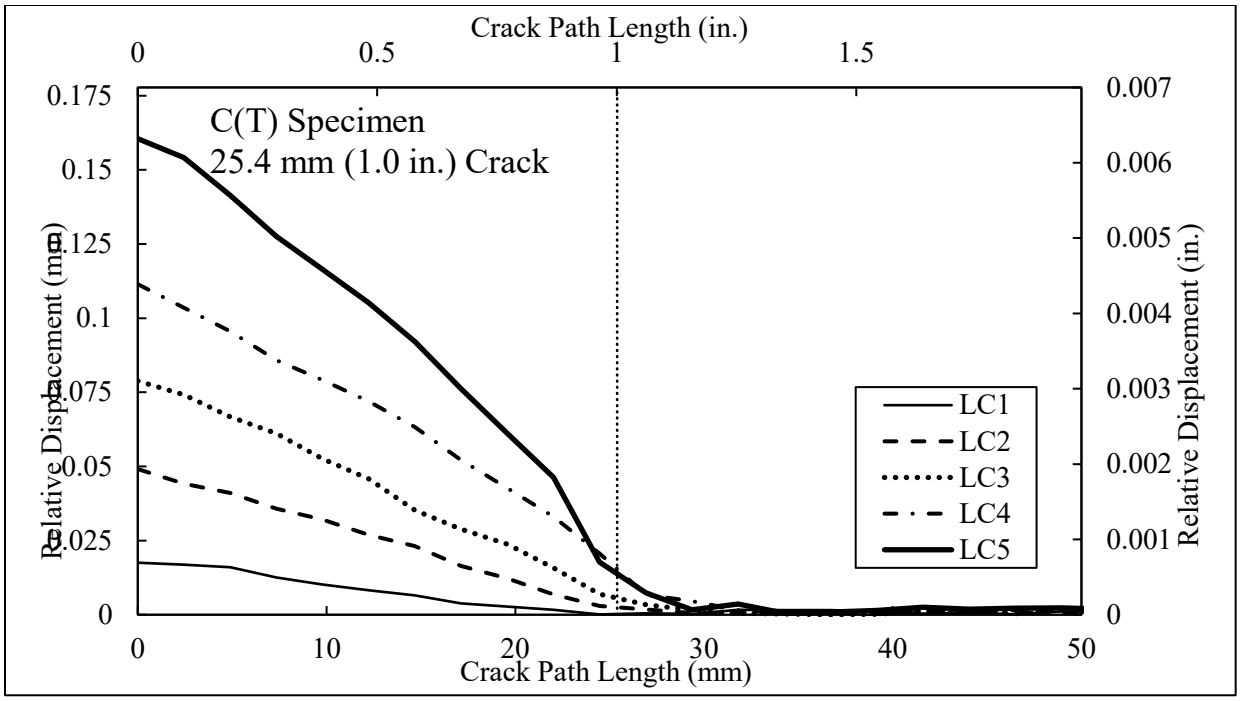

Figure 2.4 Relative displacement along crack path for 25.4 mm (1.0 in.) cracked in-plane specimen

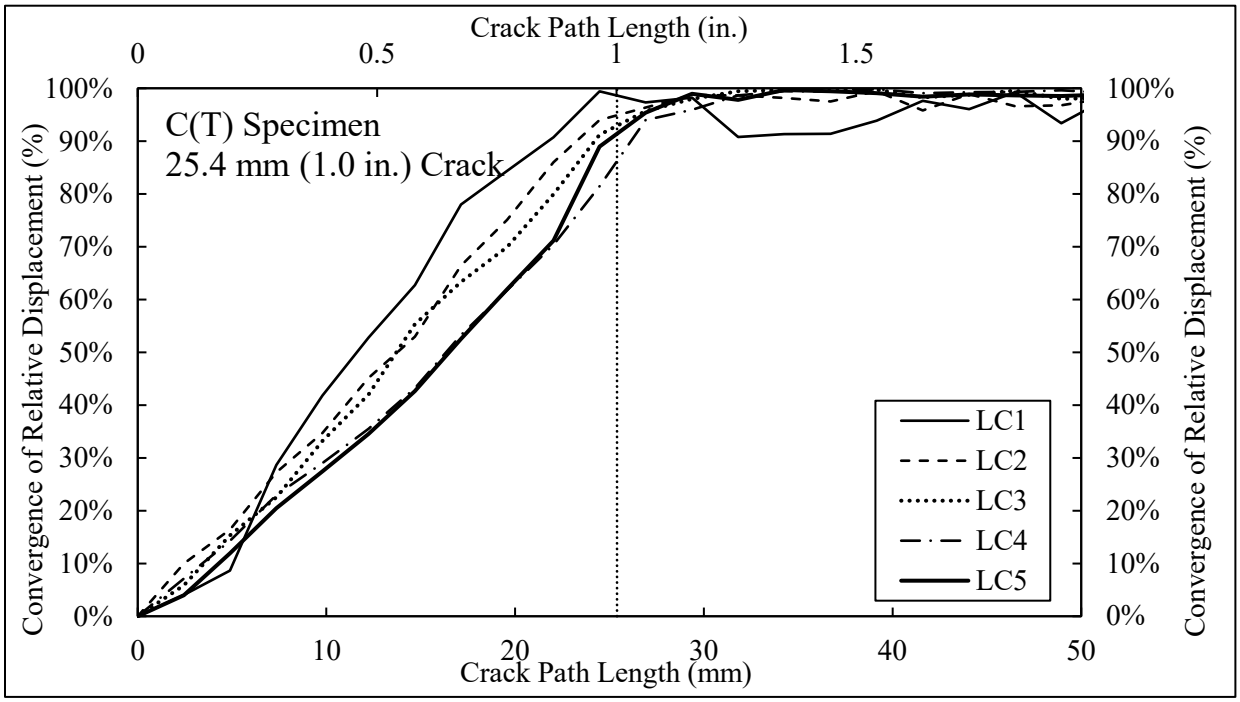

Figure 2.5 Convergence of relative displacement for 25.4 mm (1.0 in.) cracked in-plane specimen

Table 2.2 Convergence of in-plane specimens for multiple crack lengths

Load Case	Crack Length mm (in.)			
	12.7 (0.5)	**25.4 (1.0)**	**38.1 (1.5)**	**50.8 (2.0)**
LC1	90.9%	98.3%	98.9%	99.3%
LC2	67.6%	94.7%	99.6%	99.3%
LC3	86.7%	92.9%	89.9%	99.7%
LC4	68.5%	85.8%	94.8%	97.7%
LC5	61.5%	91.2%	91.4%	95.0%

Chapter 3 Distortion-Induced Fatigue Testing

3.1 Distortion-Induced Fatigue Test Setup and Loading

3.1.1 Test Setup

After developing a crack characterization methodology using the simplified in-plane C(T) specimens, the methodology was applied to a crack developed on a half-scale girder-to-cross-frame subassembly. The test specimen was an I-shape plate girder sub-assembly, schematically represented in Figure 3.1. The sub-assembly was fabricated from A36 steel, with a half-scale girder length of 2845 mm (112 in.), a depth of 917 mm (36.1 in.), and a web thickness of 10 mm (3/8 in.). The top of the girder sub-assembly connected to the reaction floor of the laboratory, restraining the flange from out-of-plane motion, providing an approximation of the way that the axial stiffness of a concrete deck restrains out-of-plane motion on a bridge girder. At the mid-span of the girder, a cross-frame was installed and attached through a connection plate only welding to the girder web.

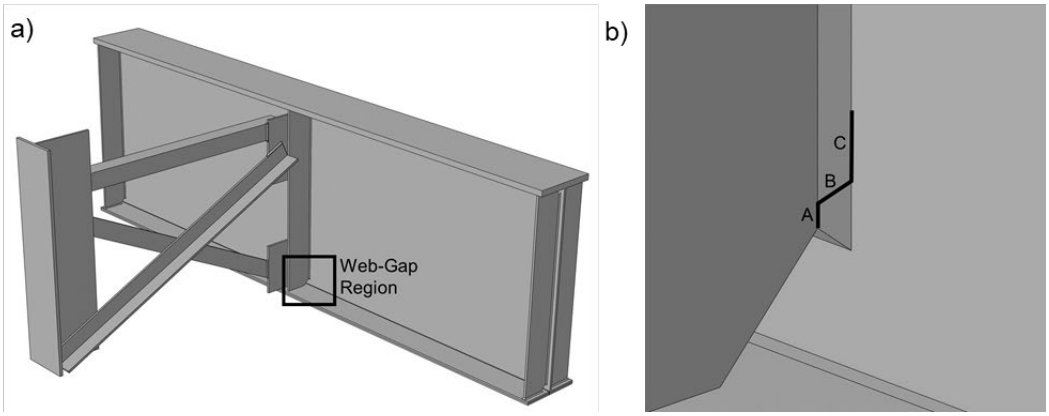

Figure 3.1 a) Out-of-plane girder subassembly and b) crack location and geometry

A vertical displacement was applied to the far end of the cross-frame, causing the girder to be loaded out-of-plane, producing distortion-induced fatigue. Fatigue cracking was initiated in

the web-gap region between the connection plate and the flange, represented in Figure 3.1b. Prior to data collection, a fatigue crack was initiated and propagated on the girder by loading for 21,000 cycles at a load range of 2.2 to 25.5 kN (0.5 to 5.75 kips). The resulting crack was visually inspected to span between the connection plate weld and the girder web, containing two vertical segments connected by a small diagonal segment and was measured to have a crack length of 44.5 mm (1.75 in.). Each crack segment was idealized as linear and assigned a letter designation, shown in Figure 3.1b. The dimensions of each segment were A = 9.7 mm (0.38 in.), B = 14.2 mm (0.56 in.), and C = 20.6 mm (0.81 in.).

3.1.2 Test Loading Protocol

A loading protocol of varying and realistic loads was developed for the out-of-plane testing, simulating the varying traffic loads. Appropriate loading levels was determined using a finite element bridge model based on the full-scale proportions of the testing setup. After applying the AASHTO fatigue truck, realistic differential vertical deflections between adjacent girders were determined. On a full-scale model, the differential deflection was 2.54 mm (0.1 in.), so the target deflection for the half-scale model was 1.25 mm (0.05 in.). This deflection corresponded to an actuator load of 6.6 kN (1.5 kips). Seven load cases were defined for loads above and below the target load, ranging from 0.89 to 15.6 kN (0.2 to 3.5 kips), shown in table 3.1. A minimum applied load of 0.89 kN (0.2 kip) was applied in all load cases to simulate dead load.

Table 3.1 Out-of-plane loading cases

Load Case	Load Range, kN (kips)
LC1	0.89-2.2 (0.2-0.5)
LC2	0.89-4.4 (0.2-1.0)
LC3	0.89-6.7 (0.2-1.5)
LC4	0.89-8.9 (0.2-2.0)
LC5	0.89-11.1 (0.2-2.5)
LC6	0.89-13.3 (0.2-3.0)
LC7	0.89-15.6 (0.2-3.5)

3.1.3 DIC Configuration

The configuration of the DIC was very similar for the in-plane C(T) testing and the distortion-induced fatigue testing. The main difference was that out-of-plane testing required the use of a two-camera stereo setup and two LED lighting panels (fig. 3.2a and b). A high contrast speckle pattern was applied across the fatigue susceptible region to allow for reference points in the DIC processing (fig. 3.2c). While processing the DIC data, the web-to-flange weld was established as the x-axis, the stiffener-to-web weld marked the y-axis, and the z-axis was located along the direction of the cross-frame.

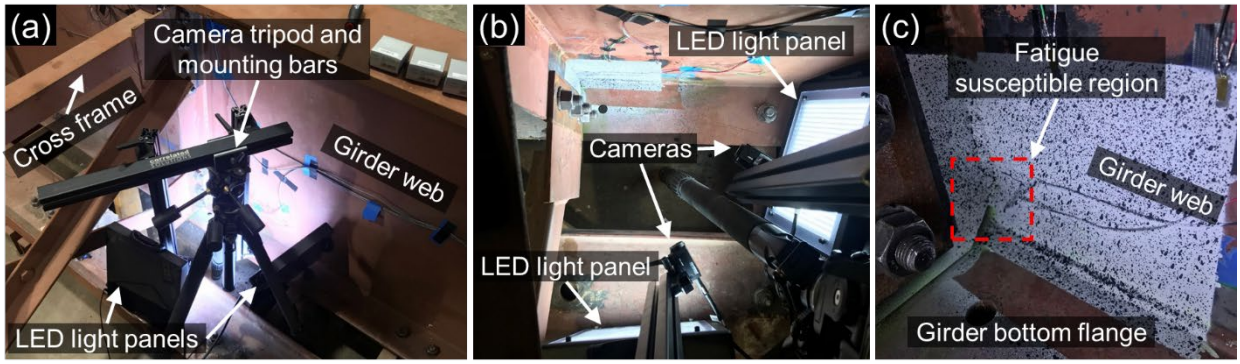

Figure 3.2 a) Hardware locations for out-of-plane testing, b) hardware orientation as seen from above, and c) fatigue susceptible region with speckle pattern applied

3.2 Crack Characterization Methodology

The methodology used to analyze in-plane specimens was applied to all distortion-induced specimens for all load cases. For analysis of distortion-induced fatigue cracks, the z-axis displacement contours were imported into an edge-detection algorithm. Despite the more complicated geometry, the crack path determined using the edge detection algorithm agreed with the location determined through visual inspection. Figure 3.3 shows typical DIC outputs in terms of strain and displacement, showing the crack path along the web gap region. All raw and DIC-analyzed photographs for the distortion-induced fatigue specimen are found in Appendix B. Orthogonal lines were drawn along the length of the crack. Relative displacements were determined for the entire length of the crack and extended past the crack tip found by the edge detection algorithm. Convergence was calculated for the crack, using equation 2.1.

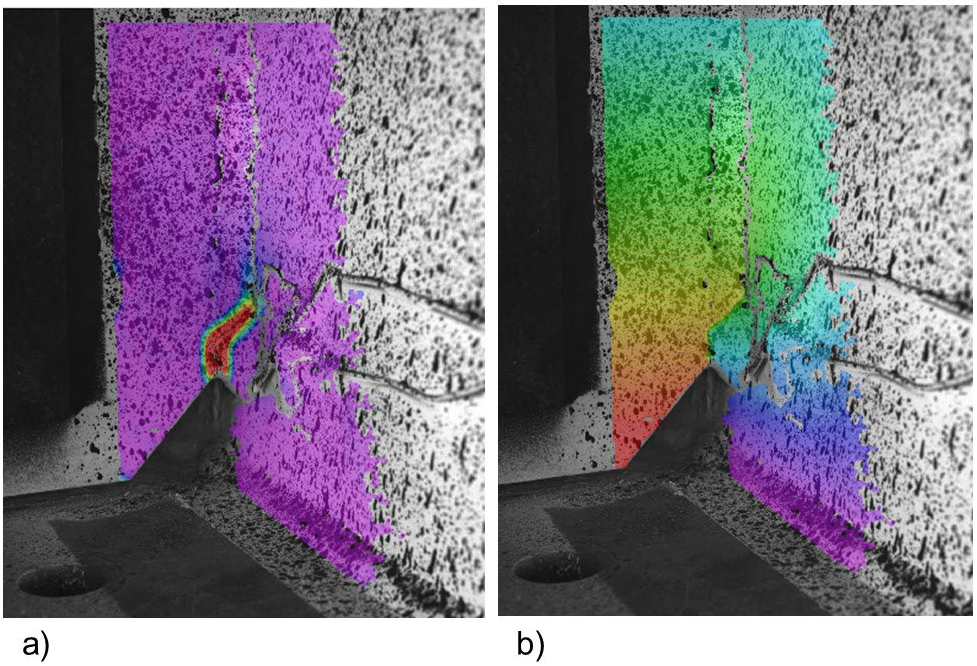

Figure 3.3 Typical DIC results showing crack location for out-of-plane testing in terms of a) strain and b) displacement

3.3 Distortion-Induced Fatigue Testing Results

Figure 3.4 shows the relative displacement of the distortion-induced fatigue specimen along the crack length for all load cases, while Figure 3.5 shows the convergence values along the crack length for load cases two through seven. The vertical dashed line indicates the visually observed crack length. The relative displacements for load case 1 were very small for the entirety of the crack length, which resulted in extreme variations of the convergence, as seen in Figure 3.6. The high variability of the convergence values indicate that the methodology developed was not applicable at this load level. This indicates that there is an applicability threshold for loading that will need to be investigated.

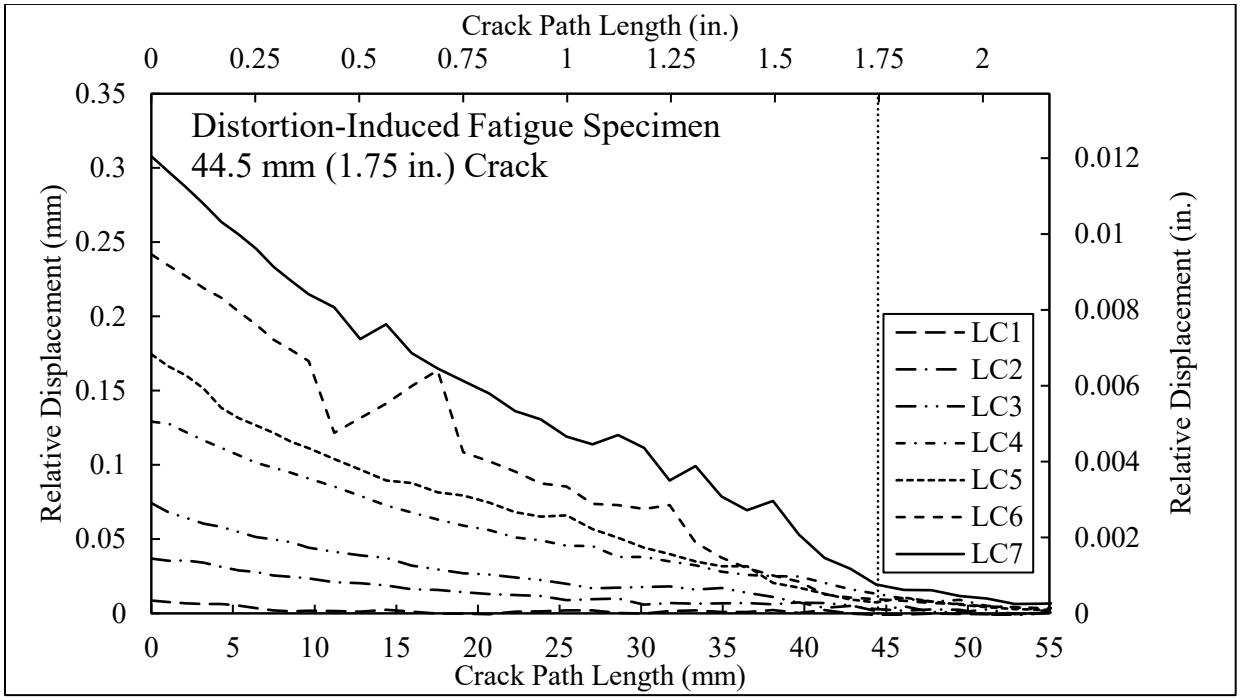

Figure 3.4 Relative displacement along the crack path length for distortion-induced fatigue specimen

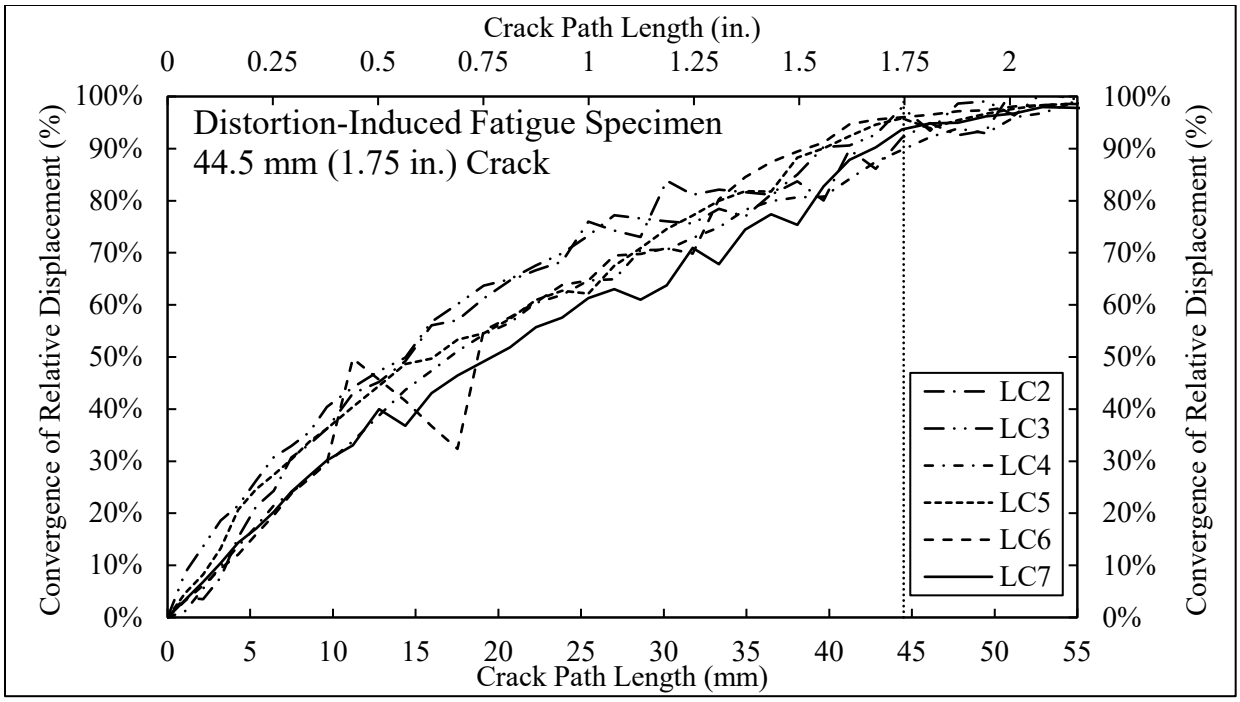

Figure 3.5 Convergence of relative displacement along the crack path length for distortion-induced fatigue specimen, excluding load case one

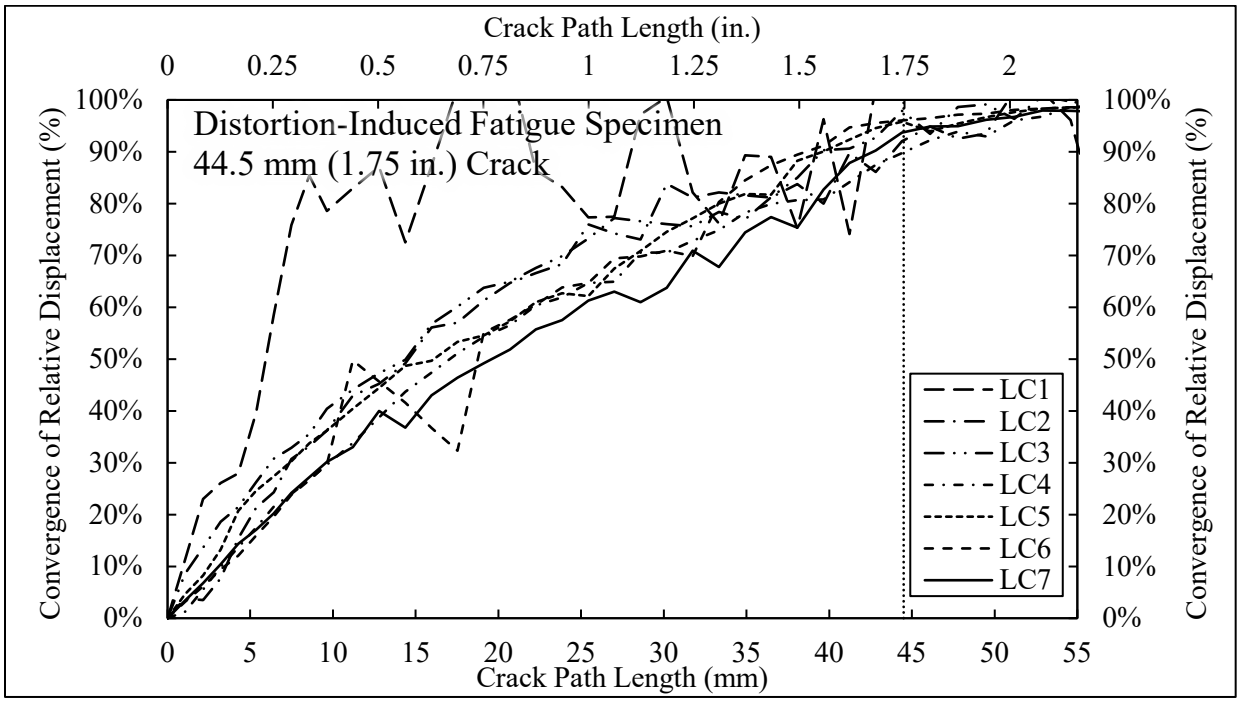

Figure 3.6 Convergence of relative displacement along the crack path length for distortion-induced fatigue specimen, including load case one

Because the C(T) specimen testing resulted in typical convergences of 90% to over 95%, those convergence values were examined for crack length prediction on the distortion-induced fatigue specimen data. Table 3.2 presents the crack length determined through convergence compared to the optically measured crack length of 44.5 mm (1.75 in.). Using 90% convergence tended to under-predict the crack length, and on average, predicted a 40.6 mm (1.59 in.) crack, which was a 9% under-prediction. The 95% convergence tended to over-predict, with an average crack length of 45.0 mm (1.77 in.), which was only 1% higher than the measured crack length.

Table 3.2 Out-of-plane crack length characterization

Load Case	**90% Convergence**		**95% Convergence**	
	Crack Length mm (in.)	**Error %**	**Crack Length mm (in.)**	**Error %**
LC1	N/A	N/A	N/A	N/A
LC2	41.2 (1.62)	-7	46.1 (1.81)	4
LC3	39.7 (1.56)	-11	43.4 (1.71)	-2
LC4	44.4 (1.75)	0	50.6 (1.99)	14
LC5	36.7 (1.44)	-18	42.8 (1.69)	-4
LC6	38.9 (1.53)	-13	51.2 (1.62)	-7
LC7	42.8 (1.69)	-4	46.1 (1.81)	4
Average	40.6 (1.59)	-9	45.0 (1.77)	1

Chapter 4 Comparison of In-plane and Distortion-Induced Results

To facilitate a comparison between the in-plane C(T) specimen results and those from the out-of-plane fatigue specimen, applied stress intensity values were calculated for the distortion-induced load cases. Finite element analyses (Alemdar et al. 2014) were used to determine Modes I, II, and III stress intensities at the crack tip for each load case, and an equivalent applied Mode I stress intensity was calculated. Modeling and data extraction techniques were validated based on known closed-form solutions of stress intensity for traditional fracture mechanics specimens (ASTM 2018). Applied stress intensity ranges for in-plane testing varied from 11 to 55 MPa√m (10 to 50 ksi√in) and values for distortion-induced fatigue testing were found to be between 10.1 and 40.5 MPa√m (9.2 and 36.9 ksi√in), providing adequate overlap to make a meaningful comparison.

Computed crack lengths were divided by the known crack lengths and plotted against applied stress intensity. This was done for each of the four in-plane crack lengths and for the distortion-induced fatigue crack. Evaluations of predicted crack length are presented for values of 90% and 95% convergence in Figure 4.1. Results of in-plane C(T) specimens are represented by the open symbols, while the distortion-induced fatigue results are represented by the filled symbols. All data points are connected with dashed lines to enhance clarity, and a solid horizontal line at 100% indicates an exact crack prediction. Data falling below the horizontal line signifies a prediction short of the physical crack length, while data above the line indicates a predicted crack length longer than the actual crack size.

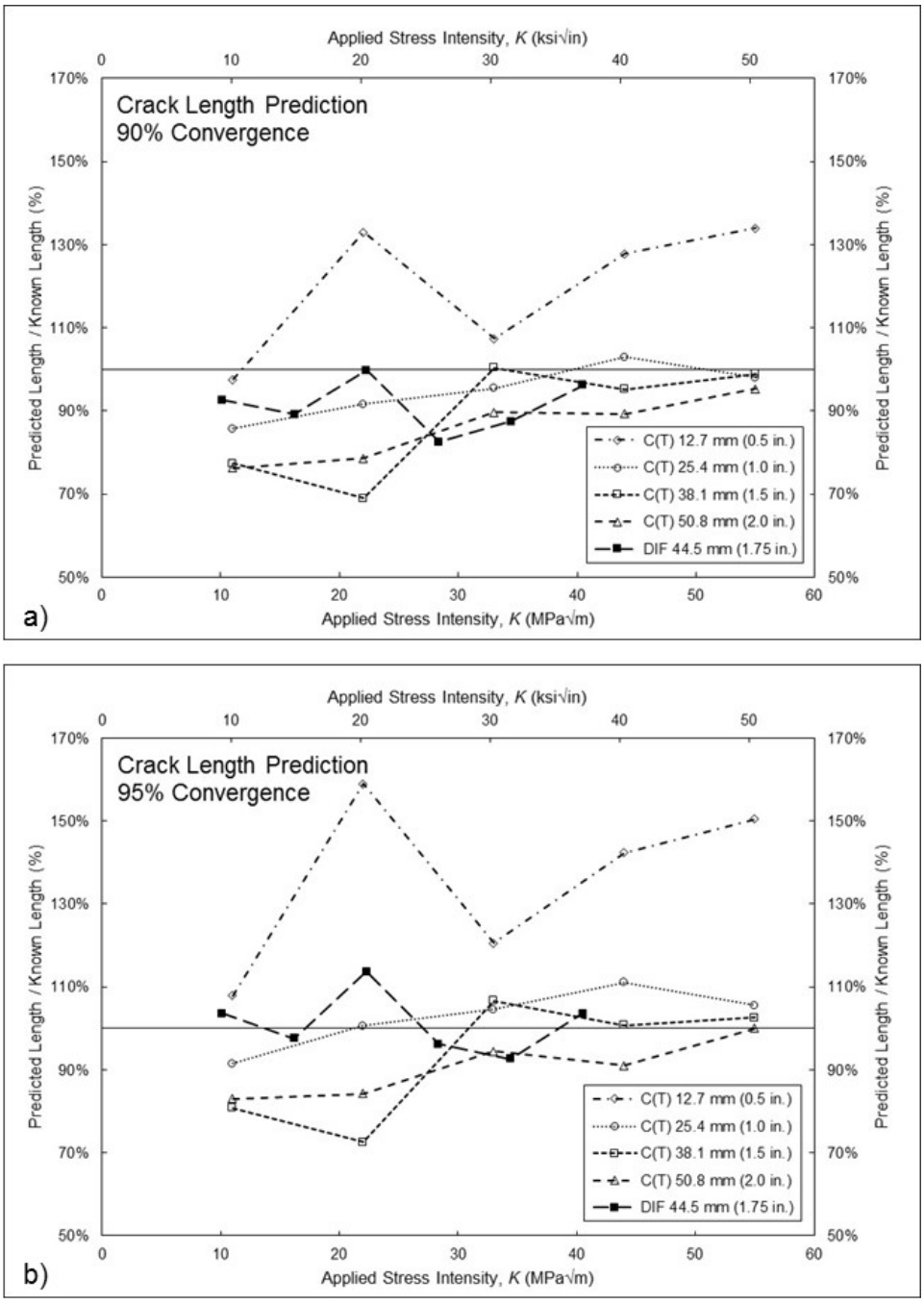

Figure 4.1 Crack length prediction at a) 90% and b) 95% convergence

Crack length predictions at both 90% and 95% convergence for the in-plane C(T) specimen with a 12.7-mm (0.5-in.) crack resulted in crack lengths longer than the physical crack size. For the majority of the in-plane specimens, however, 90% convergence resulted in crack

lengths shorter than the physical crack size. The distortion-induced fatigue results were consistent with this behavior, with all predicted crack lengths shorter than the physical crack size. Predicted crack results at 95% convergence did not exhibit a consistent trend. Disregarding the 12.7-mm (0.5-in.) specimen, half of the in-plane results over-predicted crack length at 95% convergence, while the other half under-predicted crack length. Very similar behavior was observed in the results of the out-of-plane distortion-induced fatigue specimen, with half of the load cases over-predicting and half under-predicting. In general, application of the crack characterization methodology to a distortion-induced fatigue specimen resulted in results very similar to those of the in-plane specimens, indicating that the method developed is robust enough to be applied meaningfully to realistic fatigue applications.

Chapter 5 Conclusions and Future Work

This study presented the development of a methodology for using digital image correlation data as a crack detection and characterization tool. The methodology was developed with in-plane fatigue loading data from C(T) specimens and then applied to data recorded from a distortion-induced fatigue test specimen. Edge detection algorithms were applied to DIC displacement data contours to determine the crack path, and relative displacements orthogonal to the crack path were then used to calculate a value of convergence, used to identify the crack tip. A theoretical convergence value of 100% should indicate the crack tip, where no relative displacement is occurring orthogonal to the crack path. However, results of in-plane testing indicated convergence between 90% and 95% corresponding to the actual crack length. Both the 90% and 95% convergence thresholds were investigated for the distortion-induced fatigue crack. For the load cases examined, 90% convergence resulted in a -9% error in crack length prediction, while 95% convergence produced an average crack length prediction only 1% beyond the known crack length.

The threshold of applicability with respect to load was identified on the distortion-induced fatigue specimen, as the lowest load case examined was unable to produce adequate results. However, this threshold was found to be below fatigue loads expected on steel highway bridges. Further work in determining limits of the developed methodology should be undertaken, including the physical limits of DIC to produce data that can be analyzed. This should include variations in surface condition, lighting, and camera focus. As used in this study, DIC requires a precise setup and operator interaction to provide the resolution presented. Further work is needed to develop a deployment mechanism capable of collecting DIC data with limited physical interaction, allowing for a potentially non-contact, automated inspection process. Additionally,

the ability of 2D DIC to collect data on distortion-induced fatigue cracks should be examined. Investigating additional crack lengths and complex crack geometries, such as bifurcated distortion-induced fatigue cracks, would provide further insight into the potential strengths and weaknesses of the methodology. As used in this study, DIC requires extensive setup and operator interaction to provide the resolution presented.

Although previous research has examined the applicability of DIC analyses to fatigue crack identification and characterization, the vast majority has focused on in-plane loading. Additionally, most previous analyses resulted in qualitative measures of fatigue cracks. The work presented here represents a significant advancement in this area, with quantitative crack characterization applied to out-of-plane distortion-induced fatigue cracks. Advances are necessary to develop a fully automated methodology for detecting cracks on in-service steel highway bridges. The ability to quantify and characterize distortion-induced fatigue cracks with the use of DIC data demonstrates potential for the developed methodology to be fully automated in the future, improving the practice of fatigue inspection on steel bridges.

References

Abdel-Qader, I., Abudayyeh, O., & Kelly, M. E. (2003). Analysis of edge-detection techniques for crack identification in bridges. *Journal of Computing in Civil Engineering*, 17(4), 255-263.

Alemdar, F., Overman, T., Matamoros, A., Bennett, C., and Rolfe, S. (2014). "Repairing Distortion-Induced Fatigue Cracks in Steel Bridge Girders Using Angles-with-Plate Retrofit Technique. II: Computer Simulations." *J. Struct. Eng*., 10.1061/(ASCE)ST.1943-541X.0000874.

American Society of Civil Engineers (ASCE). (2017). 2017 Infrastructure Report Card – Bridges, https://www.infrastructurereportcard.org/wp-content/uploads/2017/01/Bridges-Final.pdf

Carroll, J., Abuzaid, W., Lambros, J., Sehitoglu, H. (2012) High resolution digital image correlation measurements of strain accumulation in fatigue crack growth. Int J Fatigue. doi:10. 1016/j.ijfatigue.2012.06.010

Carroll, J., C. Efstathiou, J. Lambros, H. Sehitoglu, B. Hauber, S. Spottswood and R. Chona (2009). Investigation of fatigue crack closure using multiscale image correlation experiments. Engineering Fracture Mechanics. 76(15): 2384.

Cha, Y. J., Choi, W., & Büyüköztürk, O. (2017). Deep Learning-Based Crack Damage Detection Using Convolutional Neural Networks. *Computer-Aided Civil and Infrastructure Engineering*, 32(5), 361-378.

Chen, F. C., Jahanshahi, M. R., Wu, R. T., & Joffe, C. (2017). A texture-Based Video Processing Methodology Using Bayesian Data Fusion for Autonomous Crack Detection on Metallic Surfaces. *Computer-Aided Civil and Infrastructure Engineering*, 32(4), 271-287.

Connor, R. J., & Fisher, J. W. (2006). Identifying effective and ineffective retrofits for distortion fatigue cracking in steel bridges using field instrumentation. *Journal of Bridge Engineering*, 11(6), 745-752.

Federal Highway Administration (FHWA). (2004). *National bridge inspection standards*, Federal Register, 69 (239)

Fisher, J. W. (1984). *Fatigue and fracture in steel bridges. Case studies*.

Helfrick, M. N., Niezrecki, C., Avitabile, P., & Schmidt, T. (2011). 3D digital image correlation methods for full-field vibration measurement. Mechanical Systems and Signal Processing, 25(3), 917-927. doi:10.1016/j.ymssp.2010.08.013

Helm, J. D. (1996). Improved three-dimensional image correlation for surface displacement measurement. Optical Engineering, 35(7), 1911. doi:10.1117/1.600624

Hutt, T., and Cawley, P. (2009). Feasibility of digital image correlation for detection of cracks at fastener holes. NDT & E International. 42. 141-149. 10.1016/j.ndteint.2008.10.008.

Küntz, M., Jolin, M., Bastien, J., Perez, F., & Hild, F. (2006). Digital image correlation analysis of crack behavior in a reinforced concrete beam during a load test. Canadian Journal of Civil Engineering, 33(11), 1418-1425. doi:10.1139/l06-106

Lorenzino, P., Beretta, G., and Navarro, A. (2014). Application of Digital Image Correlation (DIC) in resonance machines for measuring fatigue crack growth. Frattura ed Integrità Strutturale. 30. 369-374. 10.3221/IGF-ESIS.30.44.

Rupil, J., Roux, S., Hild, F., and Vincent, L. (2011). Fatigue microcrack detection with digital image correlation. The Journal of Strain Analysis for Engineering Design. 46. 492-509. doi: 10.1177/0309324711402764.

Sutton, M. A., Yan, J. H., Deng, X., Cheng, C. S., and Zavattieri, P. (2007). Three-dimensional digital image correlation to quantify deformation and crack-opening displacement in ductile aluminum under mixed-mode I/III loading. Optical Engineering, 46(5), 051003. doi:10.1117/1.2741279

Vanlanduit, S., Vanherzeele, R., Longo, R., and Guillaume, P. (2008). Investigation of fatigue cracks using digital image correlation. Emerging Technologies in NDT. 4. 53-58.

Whitehead, J. (2015). "Probability of detection study for visual inspection of steel bridges." Master's Thesis, Purdue University, West Lafayette, IN.

Yamaguchi, T., & Hashimoto, S. (2010). Fast crack detection method for large-size concrete surface images using percolation-based image processing. *Machine Vision and Applications*, 21(5), 797-809.

Yeum, C. M., & Dyke, S. J. (2015). Vision-based automated crack detection for bridge inspection. *Computer-Aided Civil and Infrastructure Engineering*, 30(10), 759-770.

Yu, S. N., Jang, J. H., & Han, C. S. (2007). Auto inspection system using a mobile robot for detecting concrete cracks in a tunnel. *Automation in Construction*, 16(3), 255-261.

Yuan, Y., Huang, J., Peng, X., Xiong, C., Fang, J., & Yuan, F. (2014). Accurate displacement measurement via a self-adaptive digital image correlation method based on a weighted ZNSSD criterion. Optics and Lasers in Engineering,52, 75-85. doi:10.1016/j.optlaseng.2013.07.016

Zhang, R., & He, L. (2012). Measurement of mixed-mode stress intensity factors using digital image correlation method. Optics and Lasers in Engineering, 50(7), 1001-1007. doi:10.1016/j.optlaseng.2012.01.009

Zhao Z, and Haldar A. (1996). Bridge fatigue damage evaluation and updating using non-destructive inspections. *Engineering fracture mechanics*. 53(5), 775-88

Zhao, Y., & Roddis, W. M. K. (2004). Fatigue Prone Steel Bridge Details: Investigation and Recommended Repairs, *K-TRAN: KU-99-2, Final Report.* Kansas Department of Transportation, Topeka, KS.

Zou, Q., Cao, Y., Li, Q., Mao, Q., & Wang, S. (2012). CrackTree: Automatic crack detection from pavement images. Pattern Recognition Letters, 33(3), 227-238.

Appendix A In-Plane Testing Data and Results

Shown below are convergence of relative displacement for all testing done on the in-plane test specimen, as well as the original image compared to the strain and displacement contours.

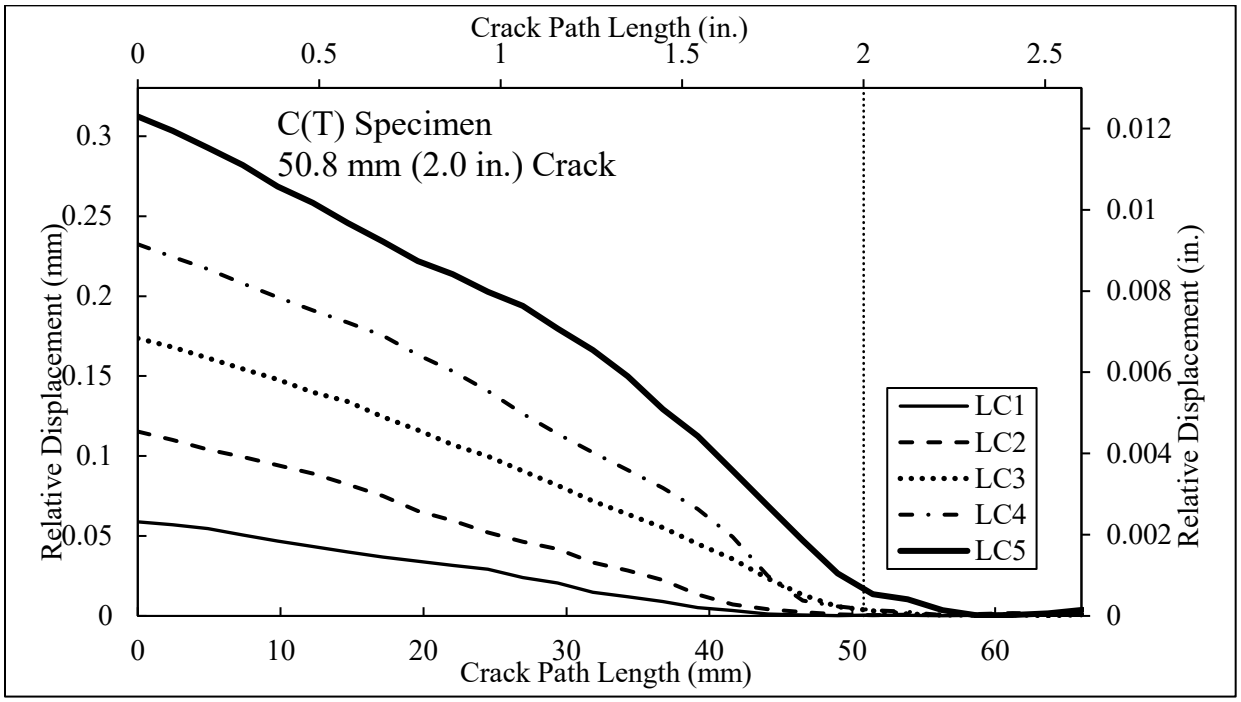

Figure A.1 Relative displacement along crack path for 50.8 mm (2.0 in.) cracked in-plane specimen

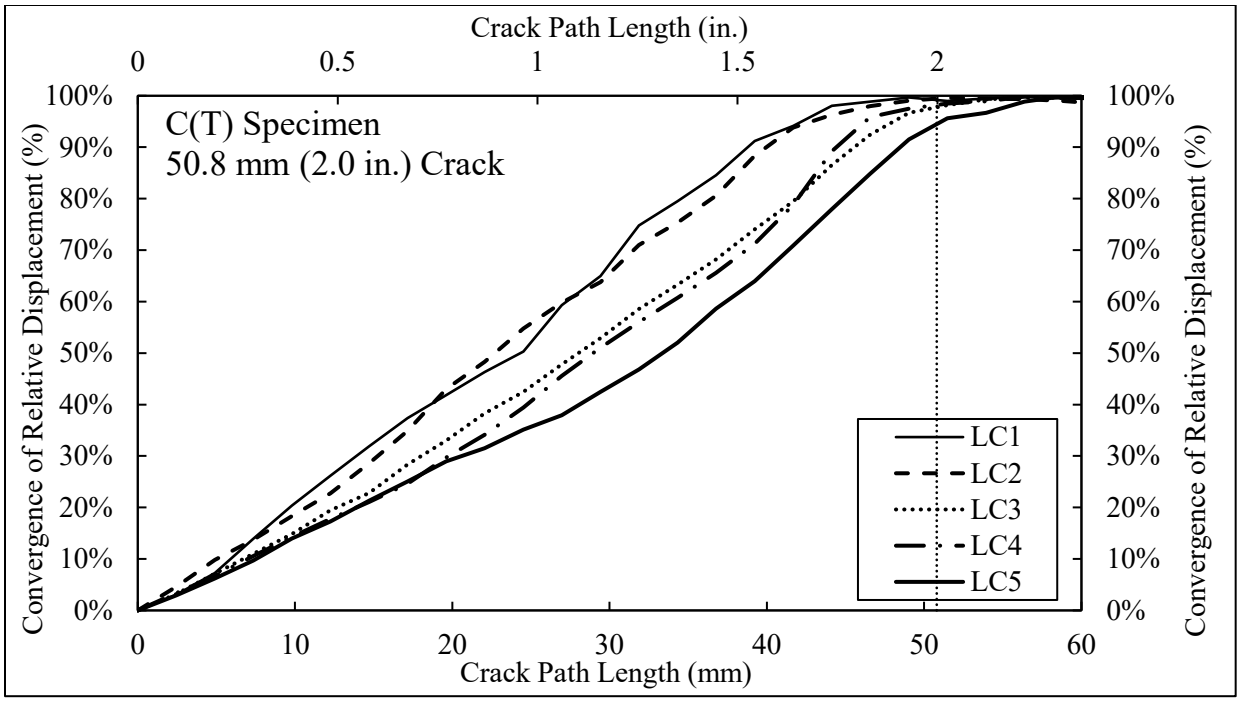

Figure A.2 Convergence of relative displacement for 50.8 mm (2.0 in.) cracked in-plane specimen

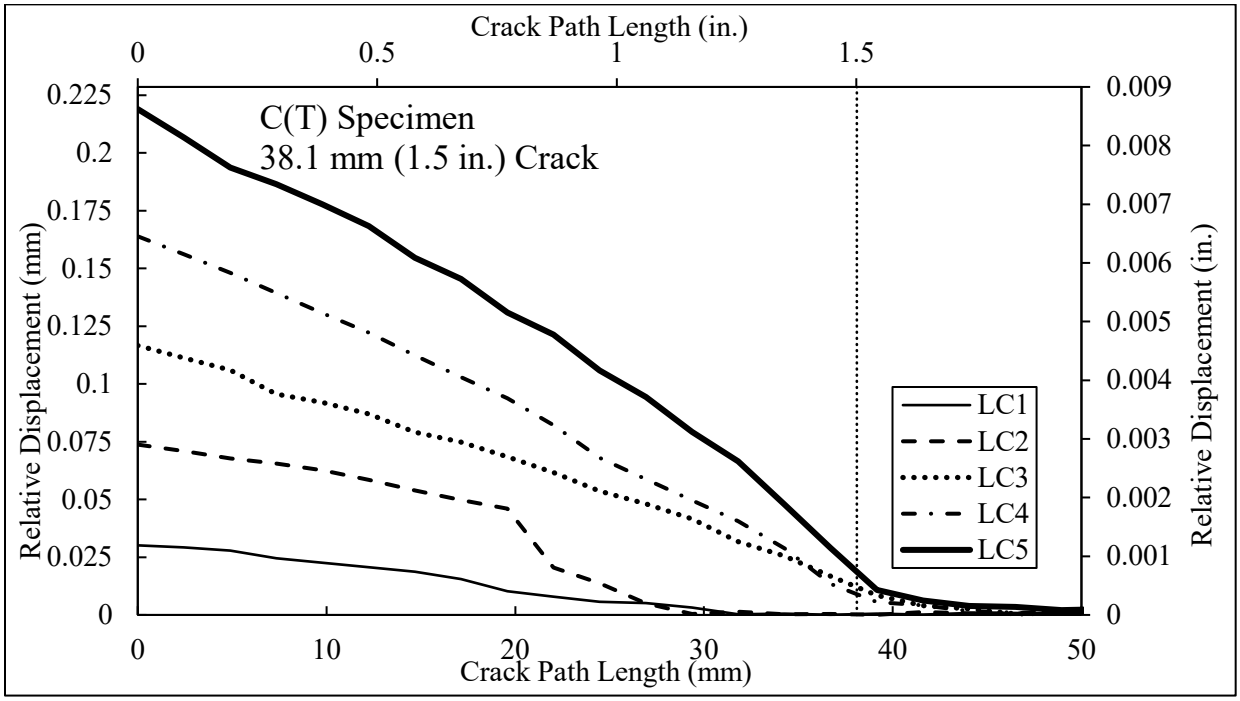

Figure A.3 Relative displacement along crack path for 38.1 mm (1.5 in.) cracked in-plane specimen

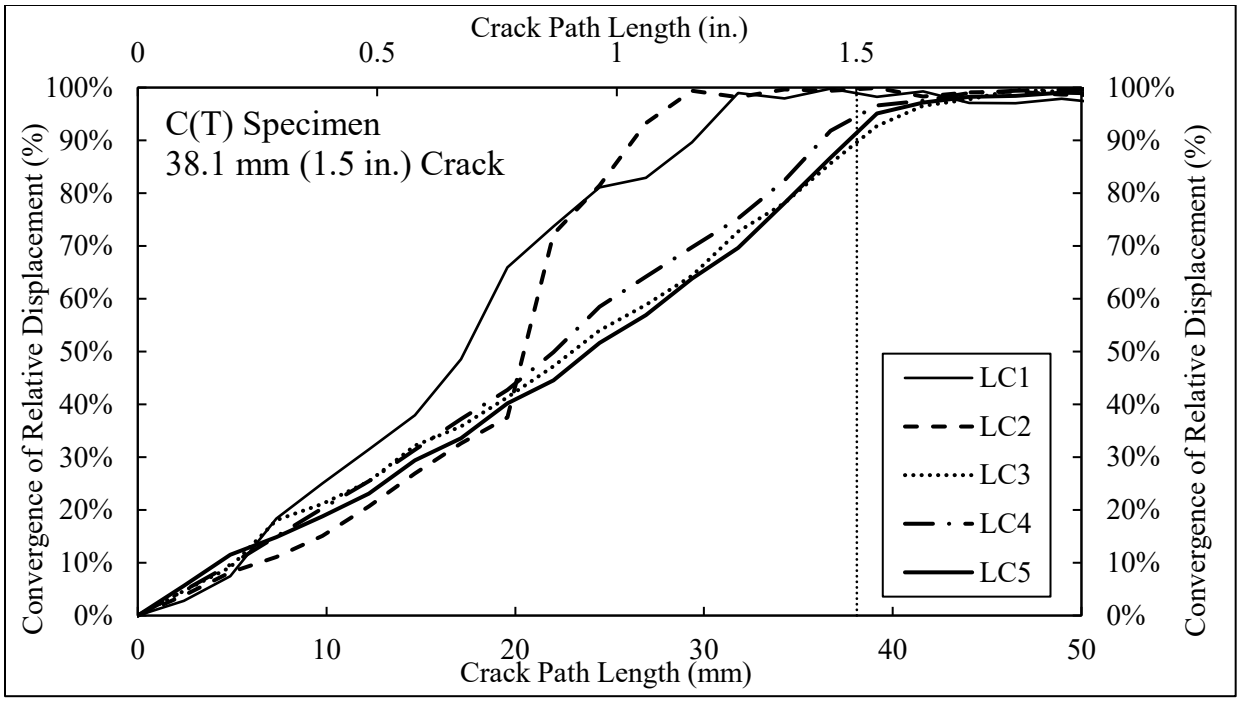

Figure A.4 Convergence of relative displacement for 38.1 mm (1.5 in.) cracked in-plane specimen

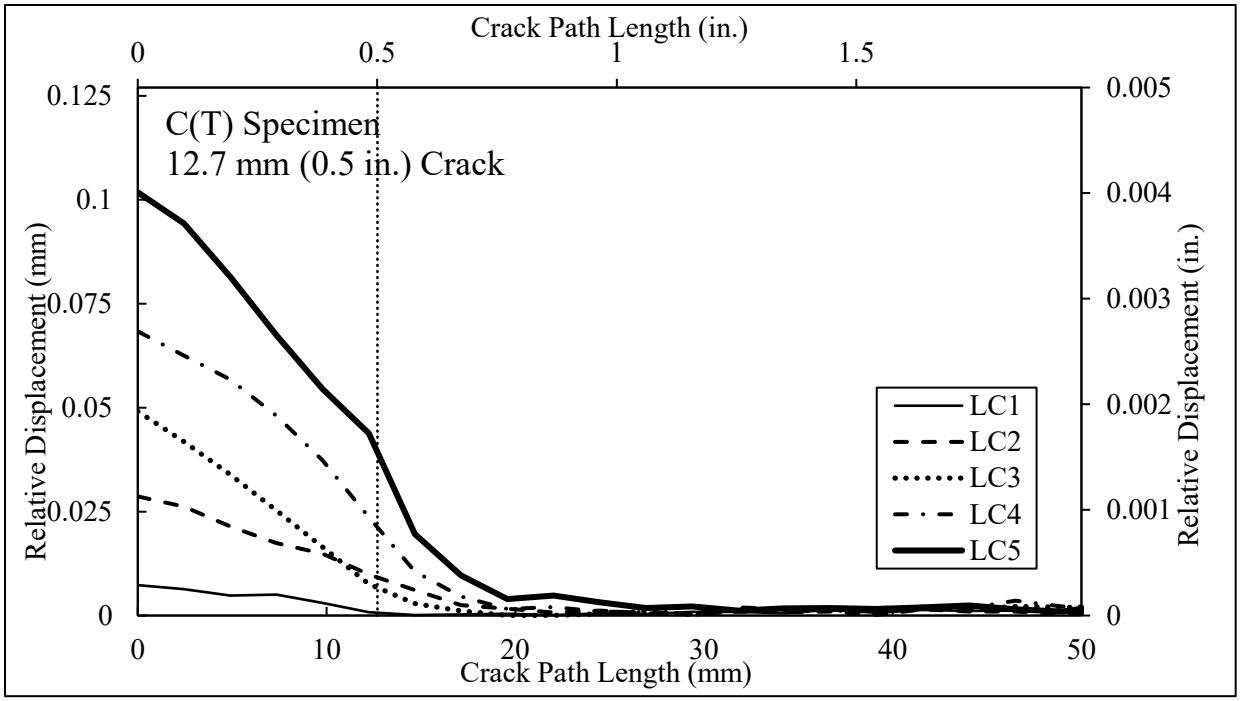

Figure A.5 Relative displacement along crack path for 12.7 mm (0.5 in.) cracked in-plane specimen

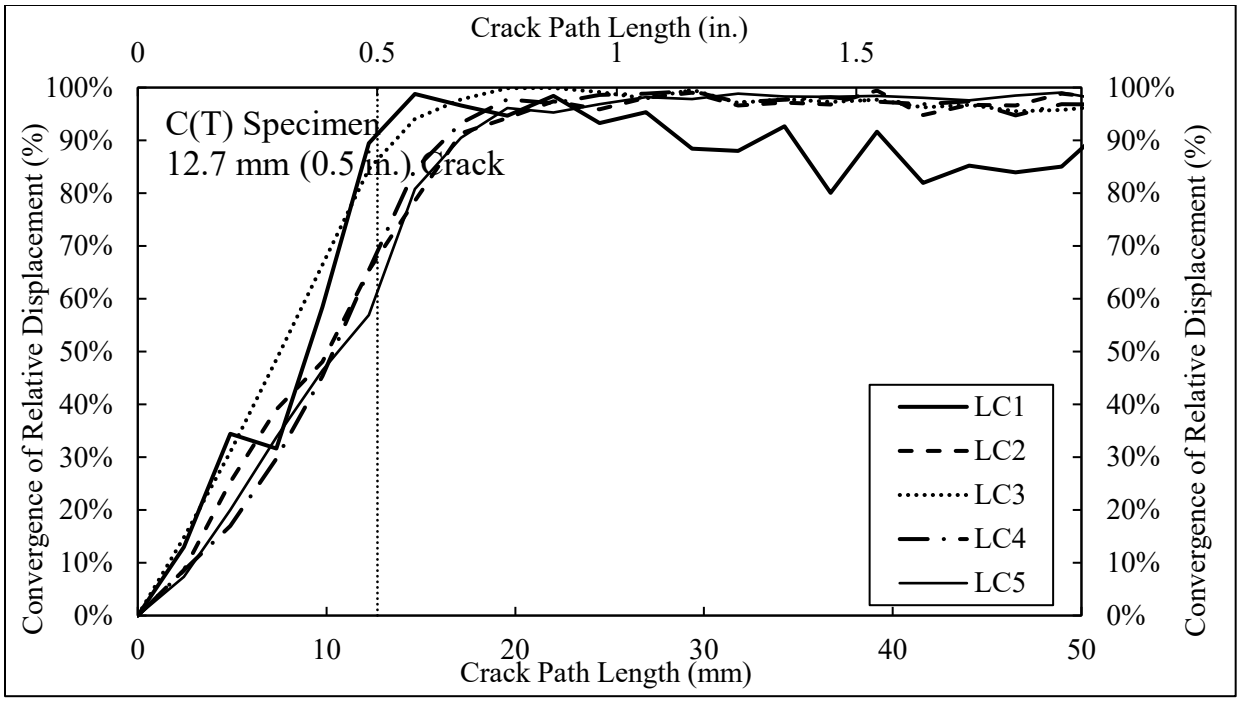

Figure A.6 Convergence of relative displacement for 12.7 mm (0.5 in.) cracked in-plane specimen

Figure A.7 Unloaded C(T) specimen with 12.7 mm (0.5 in.) in-plane crack

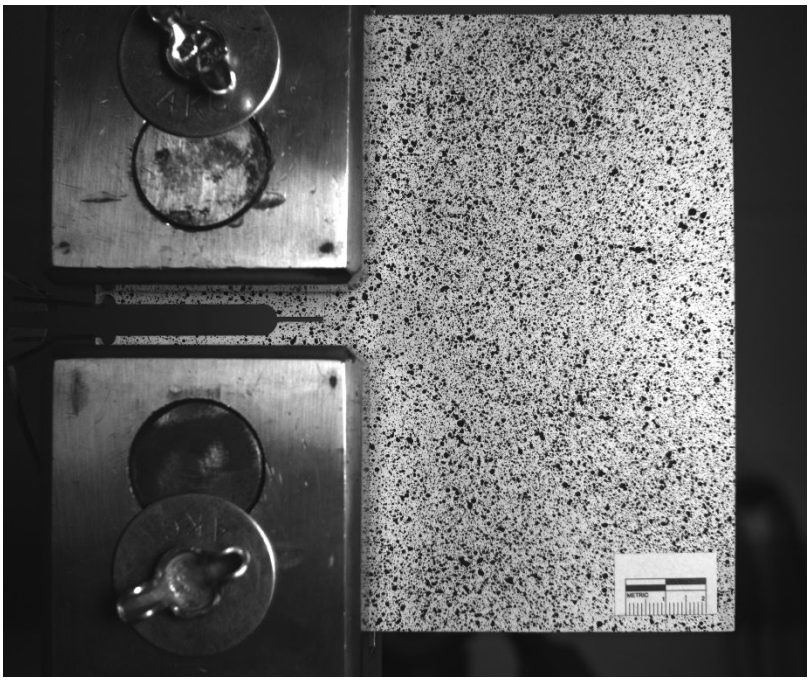

Figure A.8 C(T) specimen with 12.7 mm (0.5 in.) in-plane crack under loading case 1

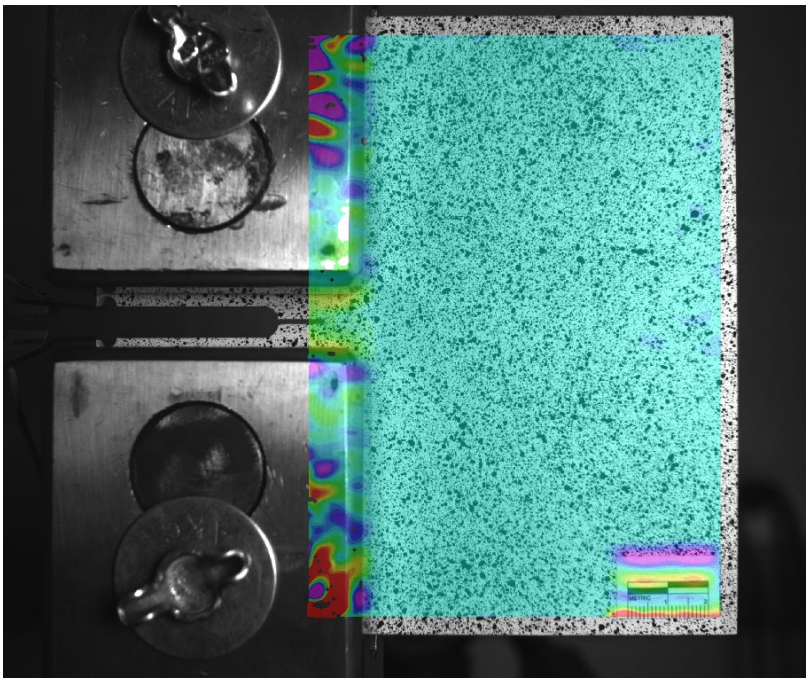

Figure A.9 Strain contours for C(T) specimen with 12.7 mm (0.5 in.) in-plane crack under loading case 1

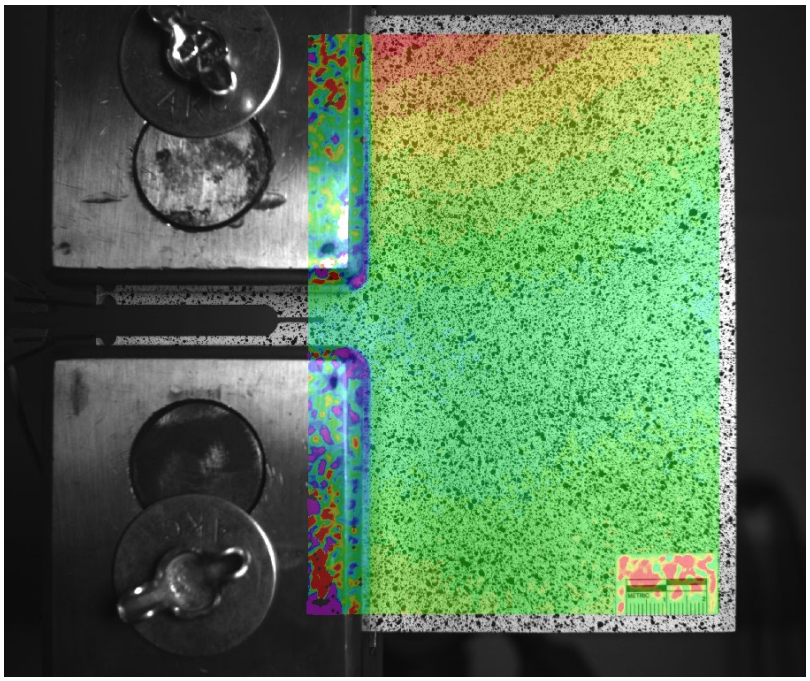

Figure A.10 Displacement contours for C(T) specimen with 12.7 mm (0.5 in.) in-plane crack under loading case 1

Figure A.11 C(T) specimen with 12.7 mm (0.5 in.) in-plane crack under loading case 2

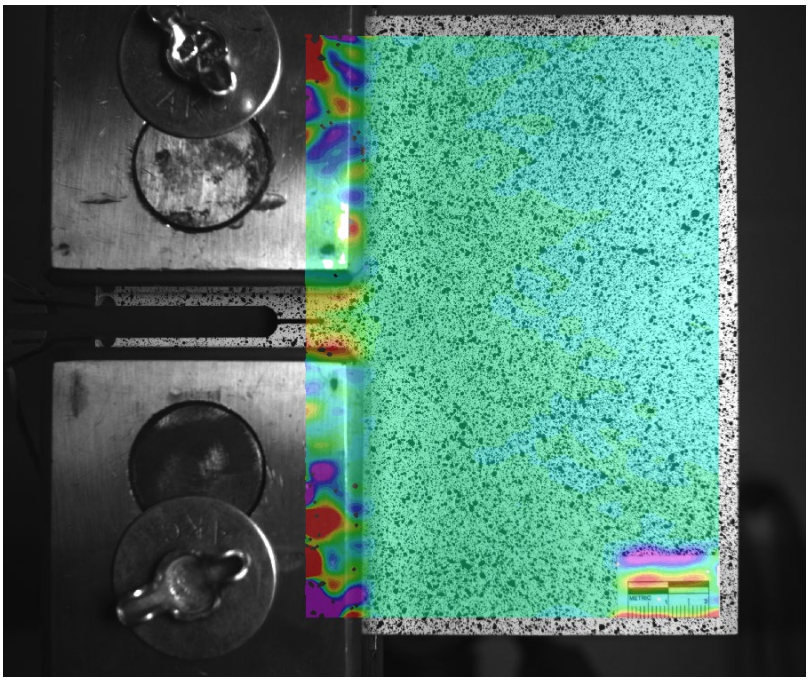

Figure A.12 Strain contours for C(T) specimen with 12.7 mm (0.5 in.) in-plane crack under loading case 2

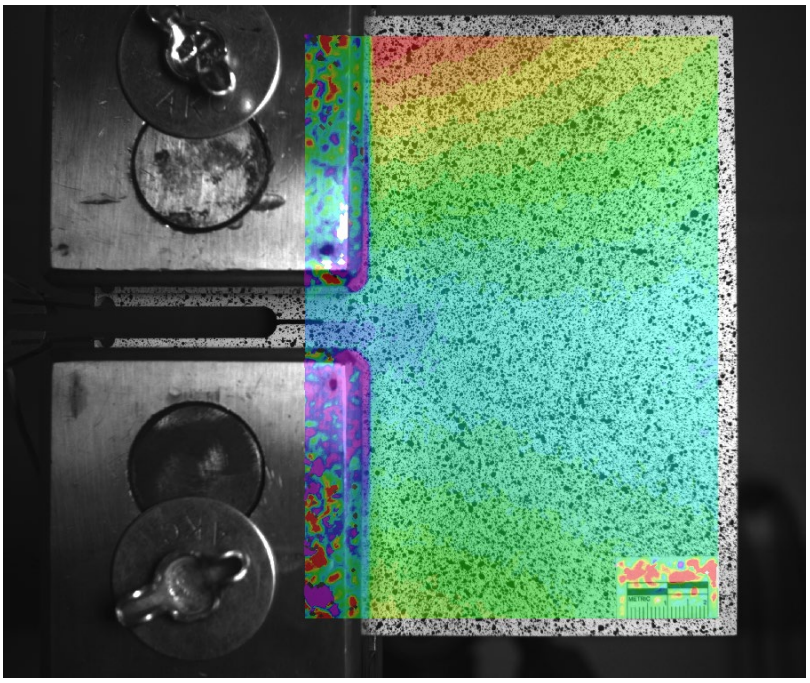

Figure A.13 Displacement contours for C(T) specimen with 12.7 mm (0.5 in.) in-plane crack under loading case 2

Figure A.14 C(T) specimen with 12.7 mm (0.5 in.) in-plane crack under loading case 3

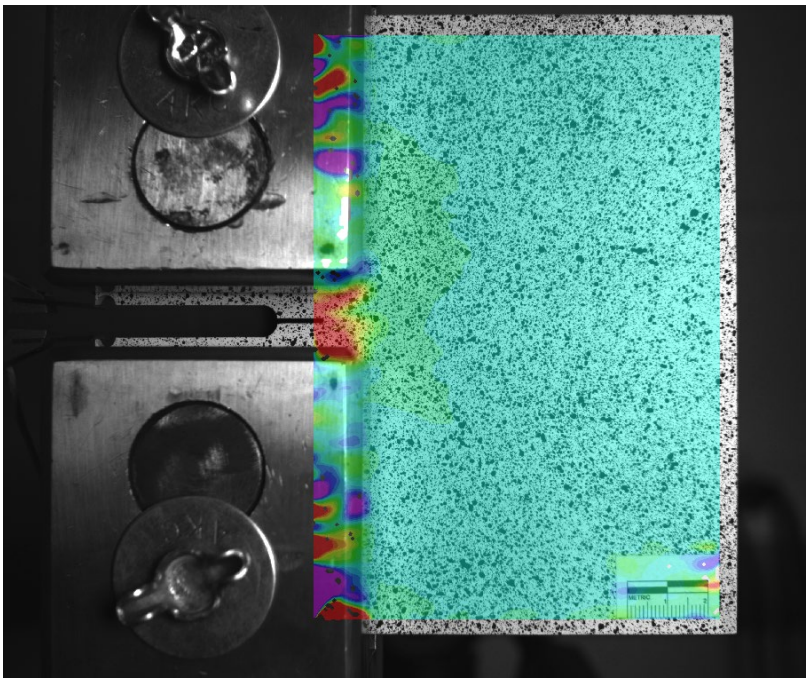

Figure A.15 Strain contours for C(T) specimen with 12.7 mm (0.5 in.) in-plane crack under loading case 3

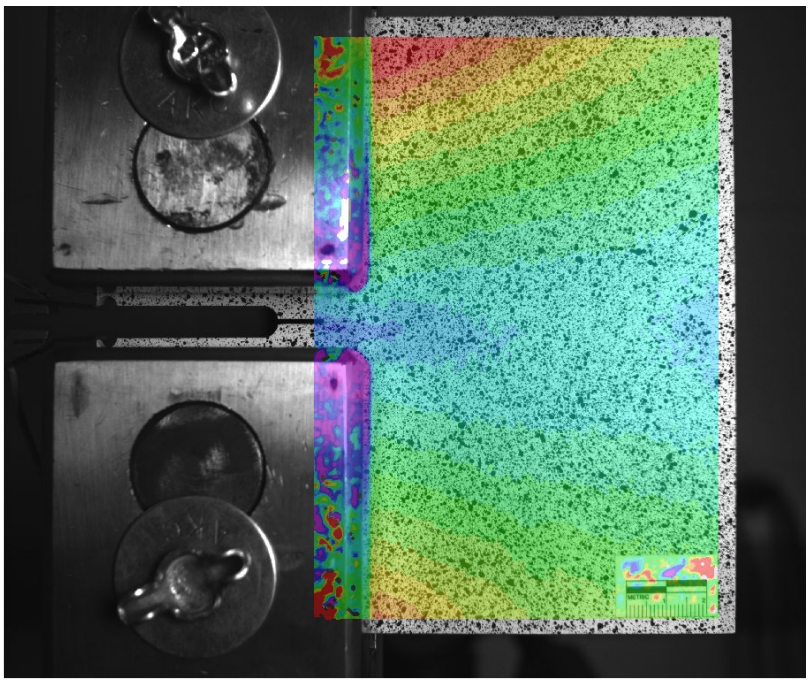

Figure A.16 Displacement contours for C(T) specimen with 12.7 mm (0.5 in.) in-plane crack under loading case 3

Figure A.17 C(T) specimen with 12.7 mm (0.5 in.) in-plane crack under loading case 4

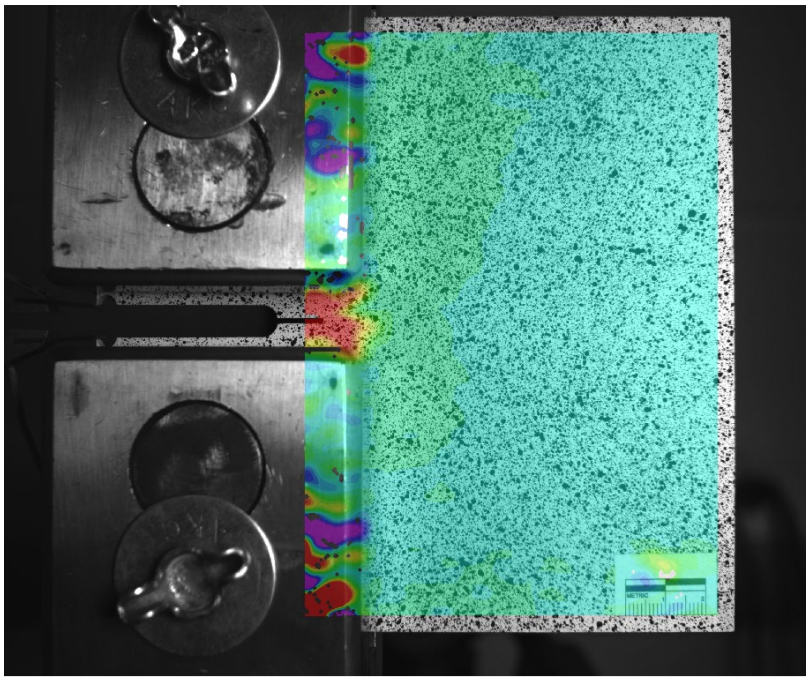

Figure A.18 Strain contours for C(T) specimen with 12.7 mm (0.5 in.) in-plane crack under loading case 4

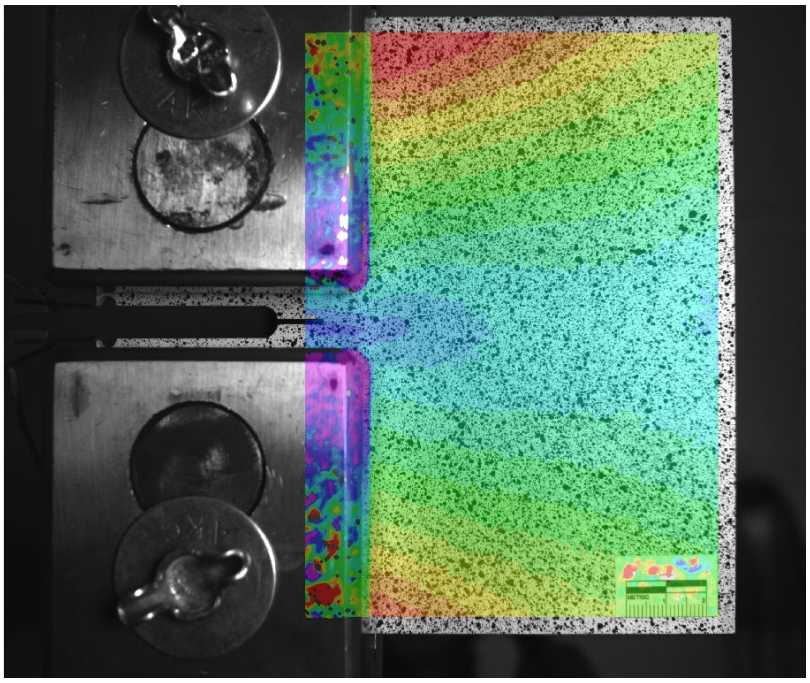

Figure A.19 Displacement contours for C(T) specimen with 12.7 mm (0.5 in.) in-plane crack under loading case 4

Figure A.20 C(T) specimen with 12.7 mm (0.5 in.) in-plane crack under loading case 5

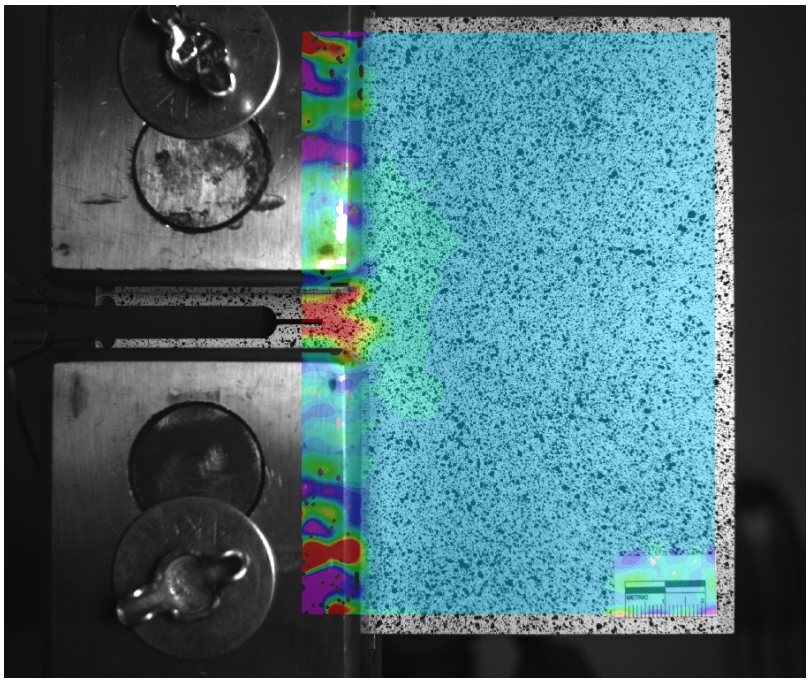

Figure A.21 Strain contours for C(T) specimen with 12.7 mm (0.5 in.) in-plane crack under loading case 5

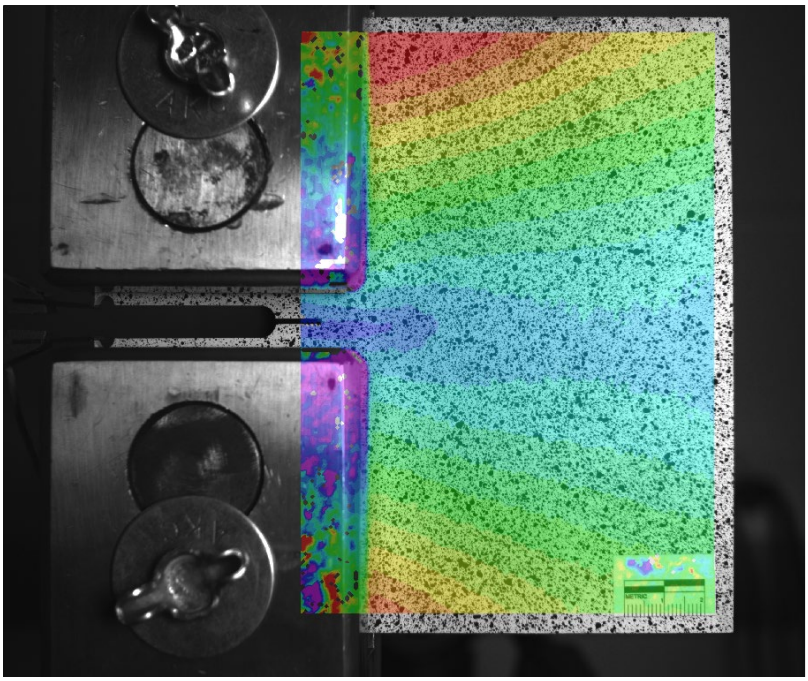

Figure A.22 Displacement contours for C(T) specimen with 12.7 mm (0.5 in.) in-plane crack under loading case 5

Figure A.23 Unloaded C(T) specimen with 24.5 mm (1.0 in.) in-plane crack

Figure A.24 C(T) specimen with 24.5 mm (1.0 in.) in-plane crack under loading case 1

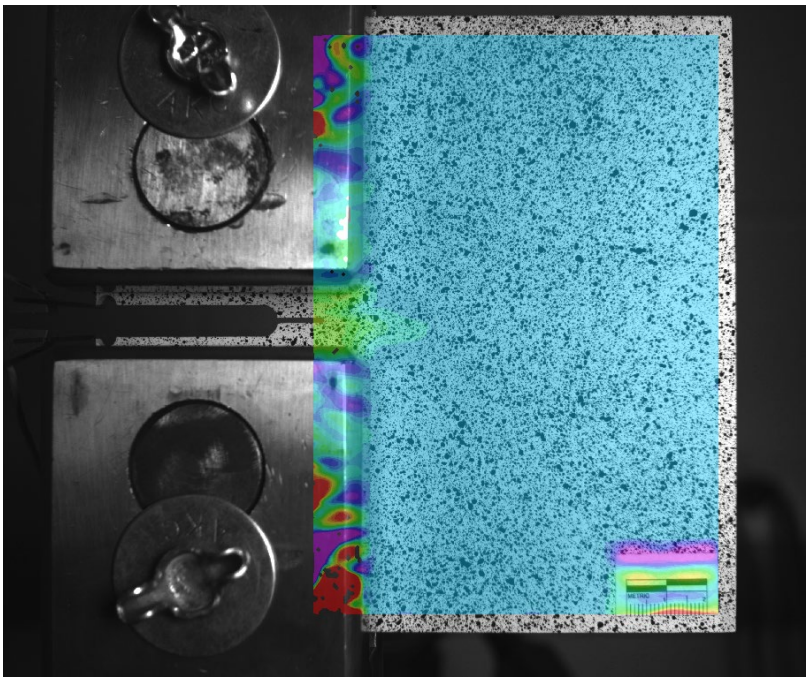

Figure A.25 Strain contours for C(T) specimen with 24.5 mm (1.0 in.) in-plane crack under loading case 1

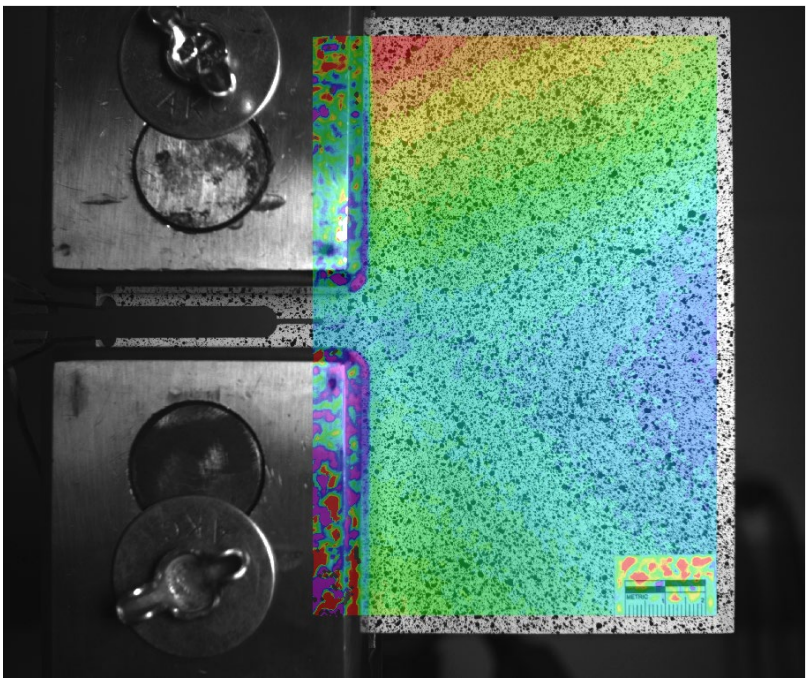

Figure A.26 Displacement contours for C(T) specimen with 24.5 mm (1.0 in.) in-plane crack under loading case 1

Figure A.27 C(T) specimen with 24.5 mm (1.0 in.) in-plane crack under loading case 2

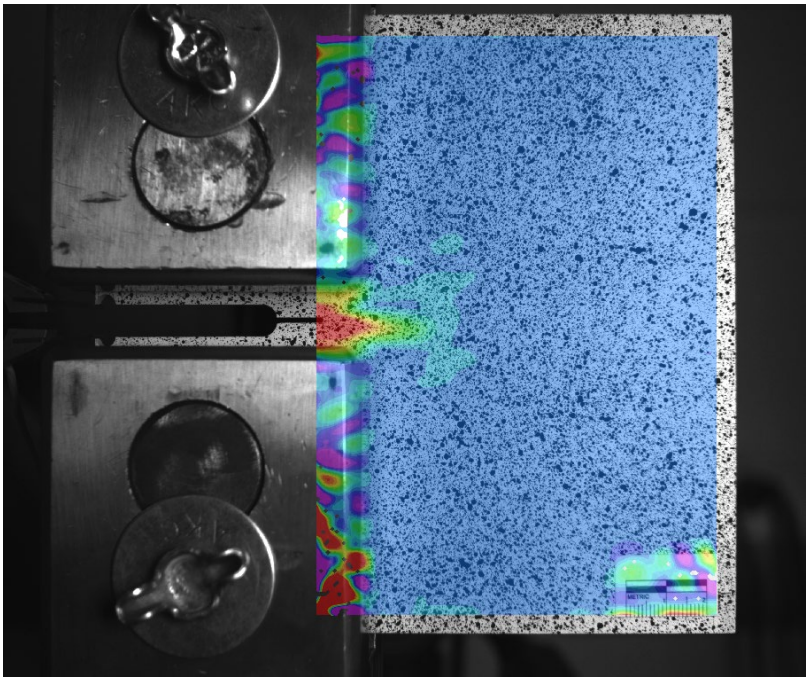

Figure A.28 Strain contours for C(T) specimen with 24.5 mm (1.0 in.) in-plane crack under loading case 2

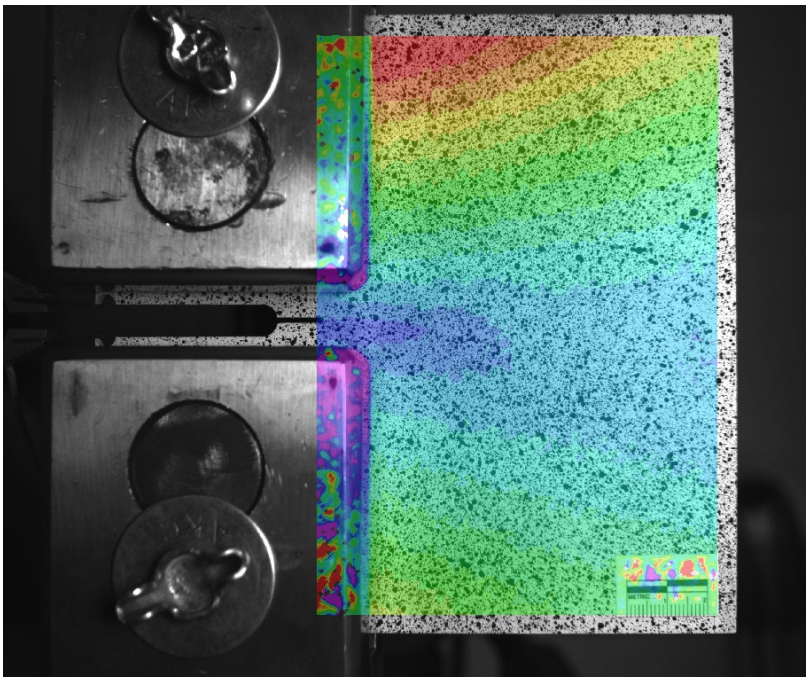

Figure A.29 Displacement contours for C(T) specimen with 24.5 mm (1.0 in.) in-plane crack under loading case 2

Figure A.30 C(T) specimen with 24.5 mm (1.0 in.) in-plane crack under loading case 3

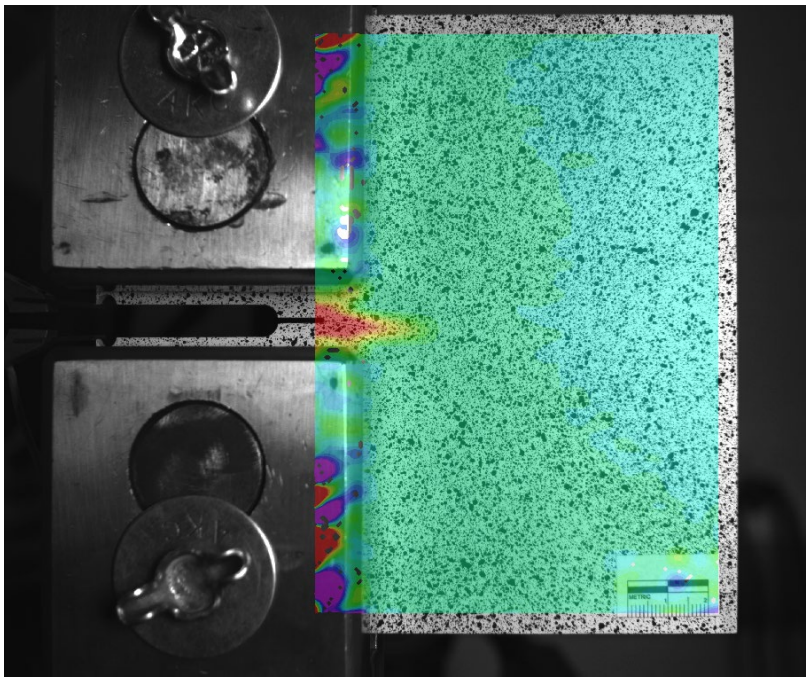

Figure A.31 Strain contours for C(T) specimen with 24.5 mm (1.0 in.) in-plane crack under loading case 3

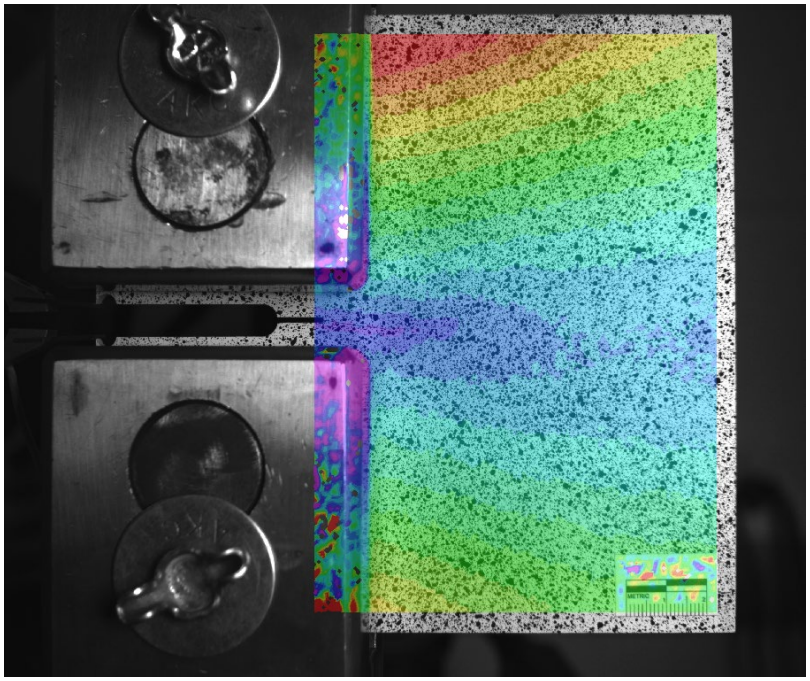

Figure A.32 Displacement contours for C(T) specimen with 24.5 mm (1.0 in.) in-plane crack under loading case 3

Figure A.33 C(T) specimen with 24.5 mm (1.0 in.) in-plane crack under loading case 4

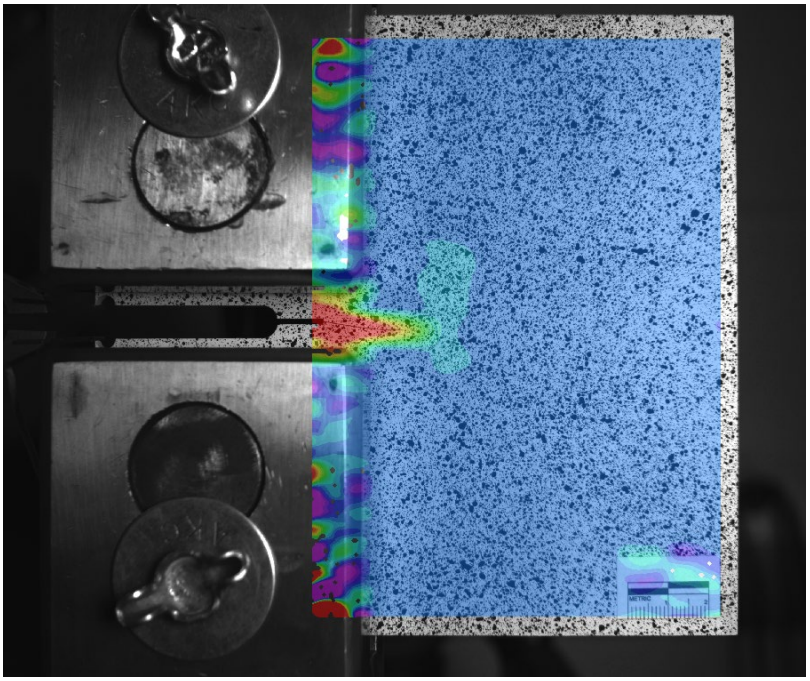

Figure A.34 Strain contours for C(T) specimen with 24.5 mm (1.0 in.) in-plane crack under loading case 4

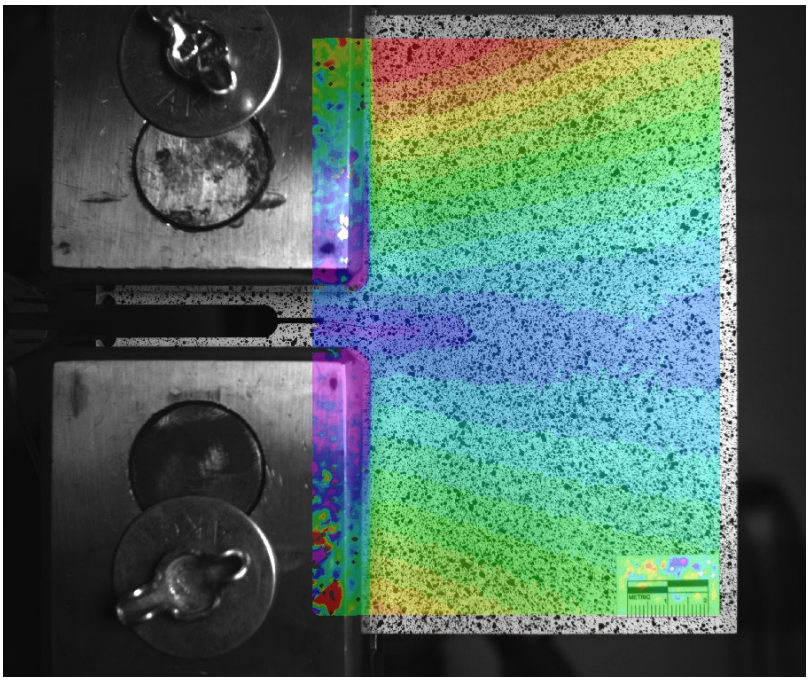

Figure A.35 Displacement contours for C(T) specimen with 24.5 mm (1.0 in.) in-plane crack under loading case 4

Figure A.36 C(T) specimen with 24.5 mm (1.0 in.) in-plane crack under loading case 5

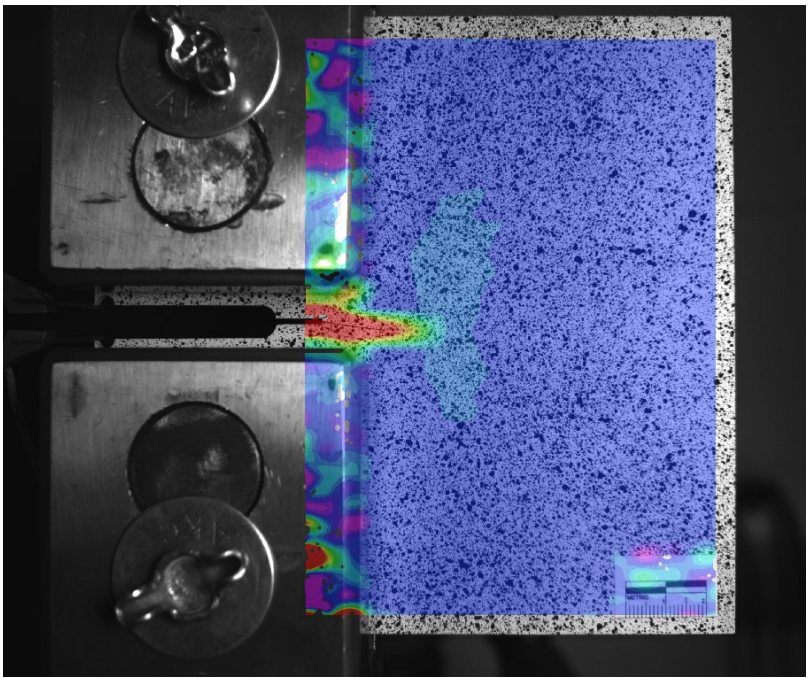

Figure A.37 Strain contours for C(T) specimen with 24.5 mm (1.0 in.) in-plane crack under loading case 5

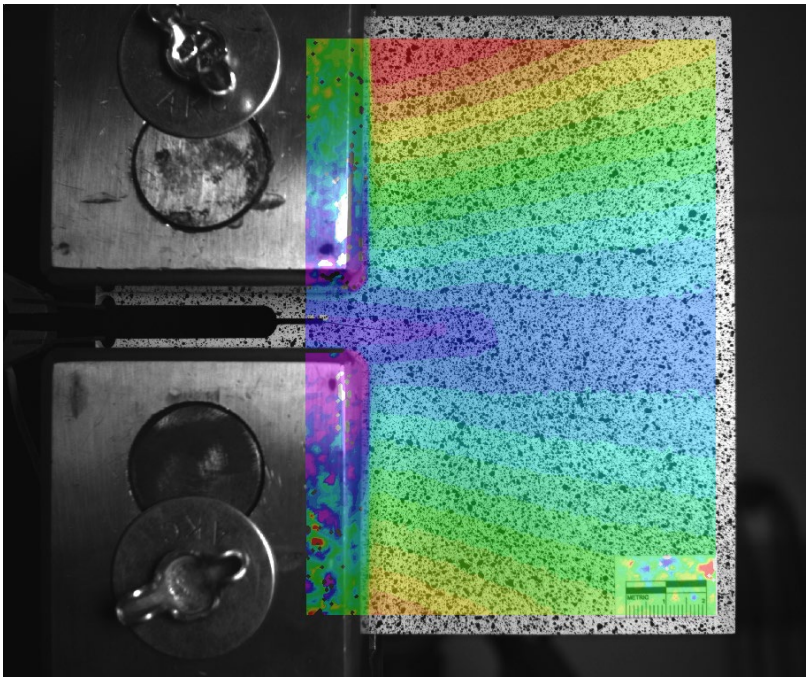

Figure A.38 Displacement contours for C(T) specimen with 24.5 mm (1.0 in.) in-plane crack under loading case 5

Figure A.39 Unloaded C(T) specimen with 38.1 mm (1.5 in.) in-plane crack

Figure A.40 C(T) specimen with 38.1 mm (1.5 in.) in-plane crack under loading case 1

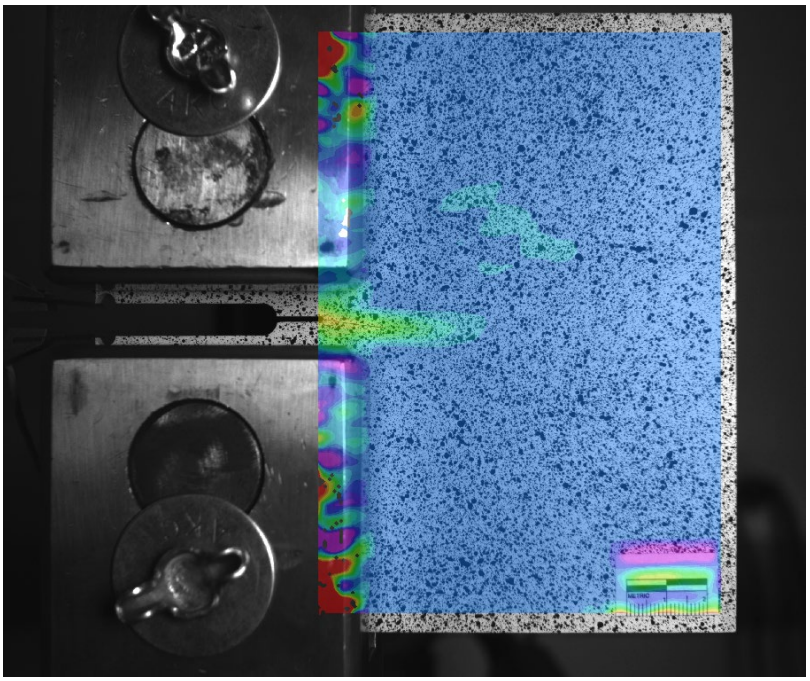

Figure A.41 Strain contours for C(T) specimen with 38.1 mm (1.5 in.) in-plane crack under loading case 1

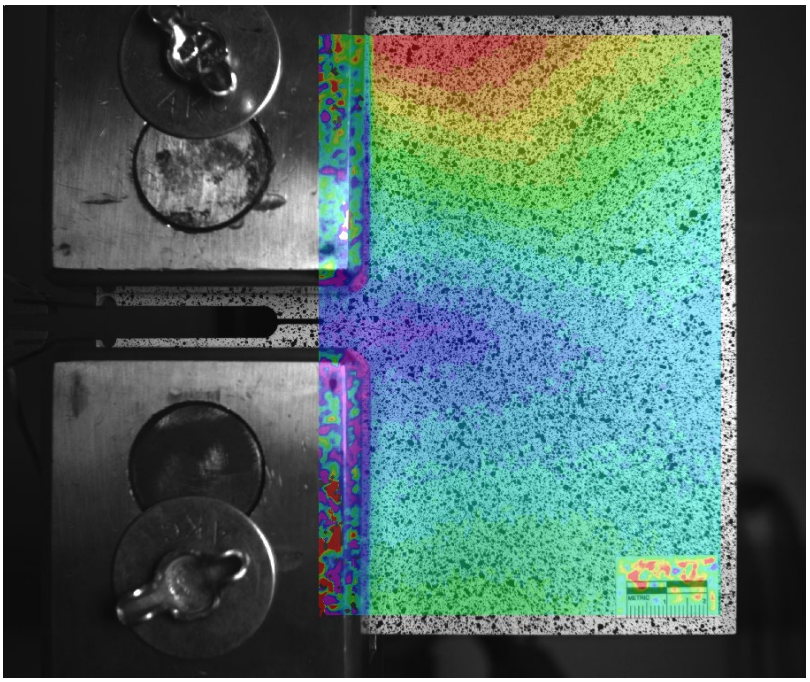

Figure A.42 Displacement contours for C(T) specimen with 38.1 mm (1.5 in.) in-plane crack under loading case 1

Figure A.43 C(T) specimen with 38.1 mm (1.5 in.) in-plane crack under loading case 2

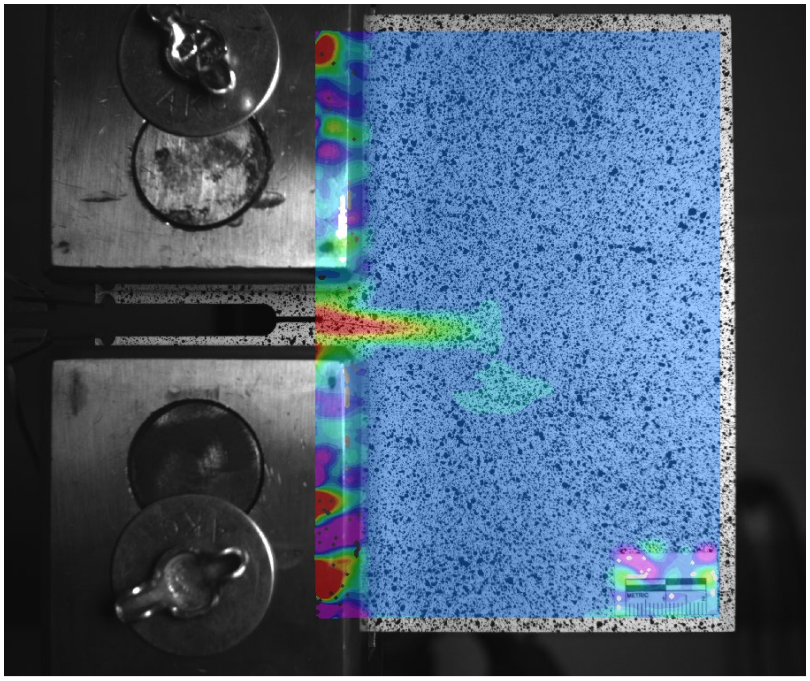

Figure A.44 Strain contours for C(T) specimen with 38.1 mm (1.5 in.) in-plane crack under loading case 2

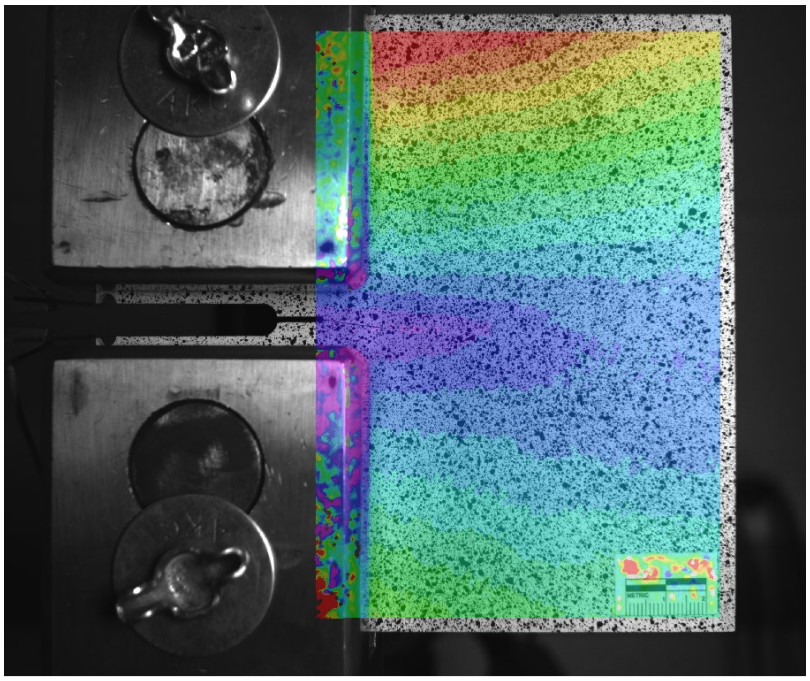

Figure A.45 Displacement contours for C(T) specimen with 38.1 mm (1.5 in.) in-plane crack under loading case 2

Figure A.46 C(T) specimen with 38.1 mm (1.5 in.) in-plane crack under loading case 3

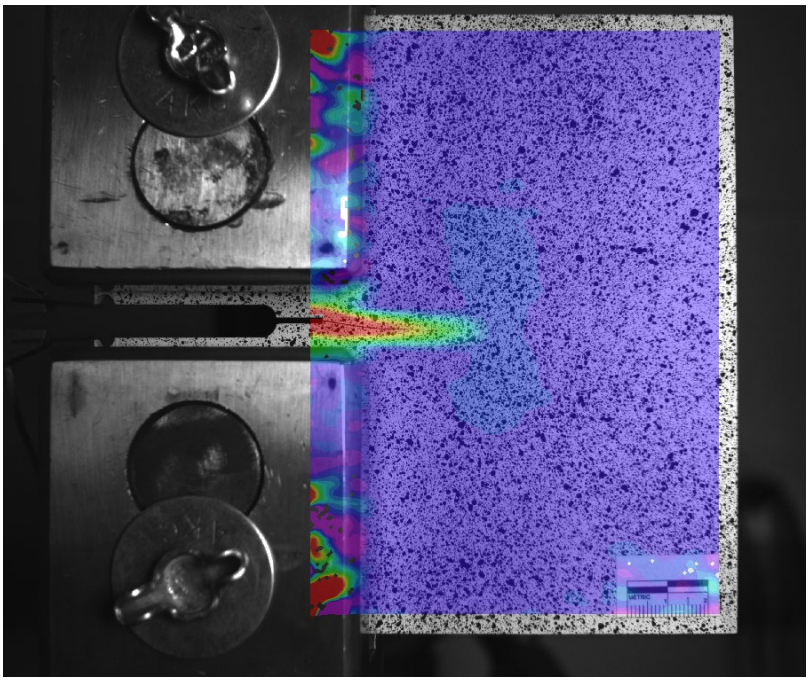

Figure A.47 Strain contours for C(T) specimen with 38.1 mm (1.5 in.) in-plane crack under loading case 3

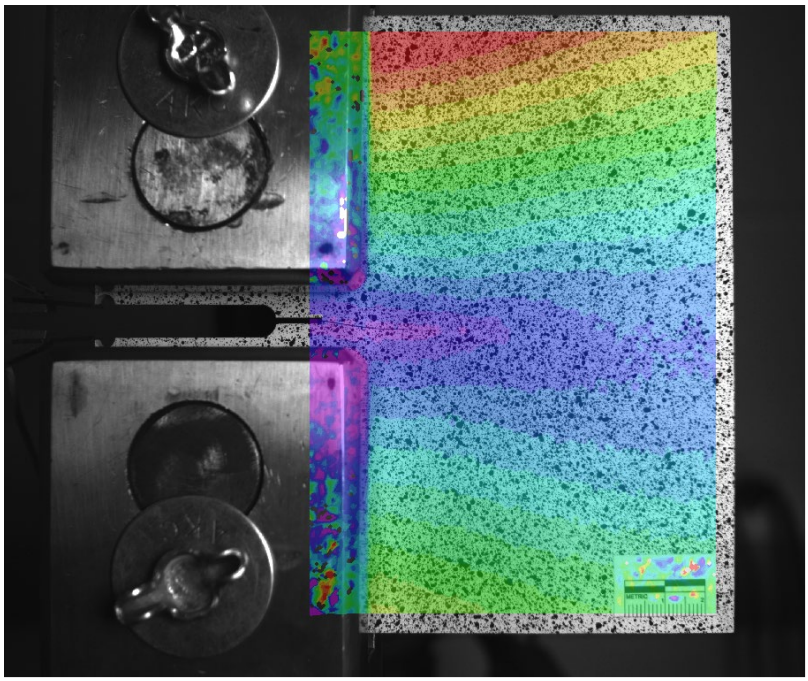

Figure A.48 Displacement contours for C(T) specimen with 38.1 mm (1.5 in.) in-plane crack under loading case 3

Figure A.49 C(T) specimen with 38.1 mm (1.5 in.) in-plane crack under loading case 4

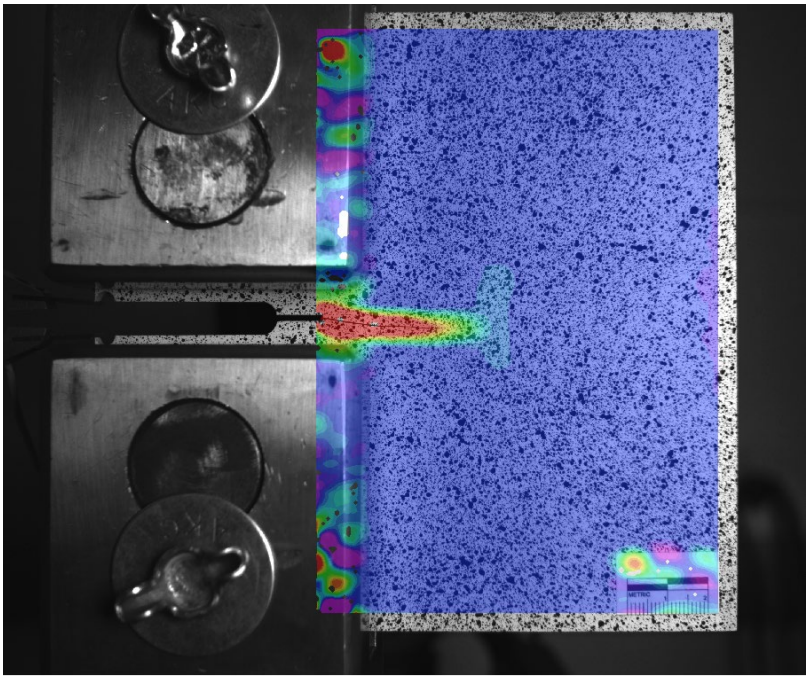

Figure A.50 Strain contours for C(T) specimen with 38.1 mm (1.5 in.) in-plane crack under loading case 4

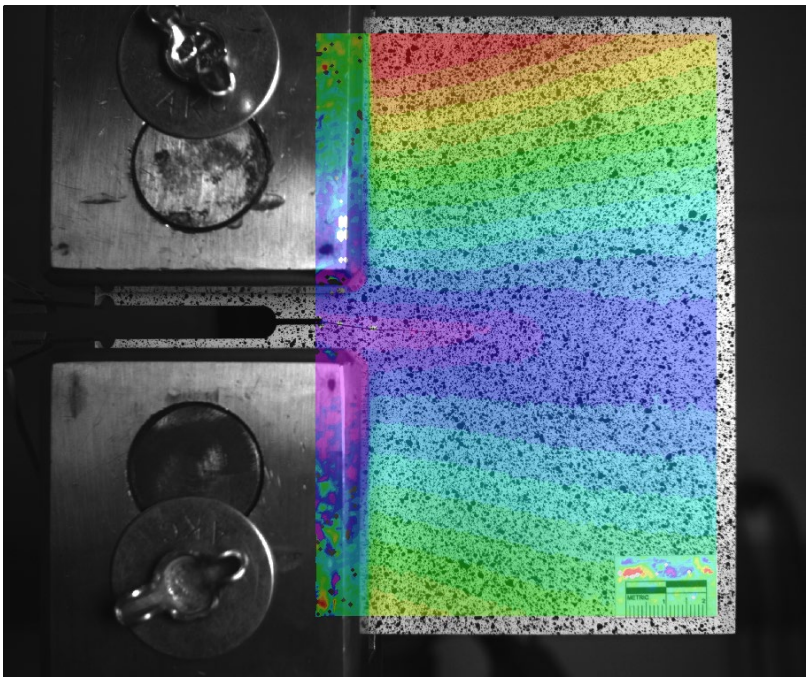

Figure A.51 Displacement contours for C(T) specimen with 38.1 mm (1.5 in.) in-plane crack under loading case 4

Figure A.52 C(T) specimen with 38.1 mm (1.5 in.) in-plane crack under loading case 5

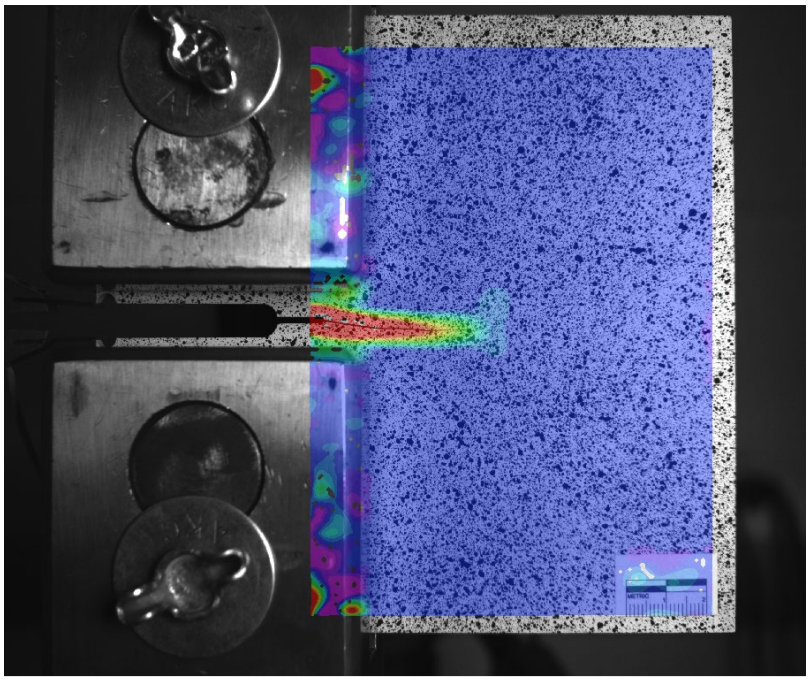

Figure A.53 Strain contours for C(T) specimen with 38.1 mm (1.5 in.) in-plane crack under loading case 5

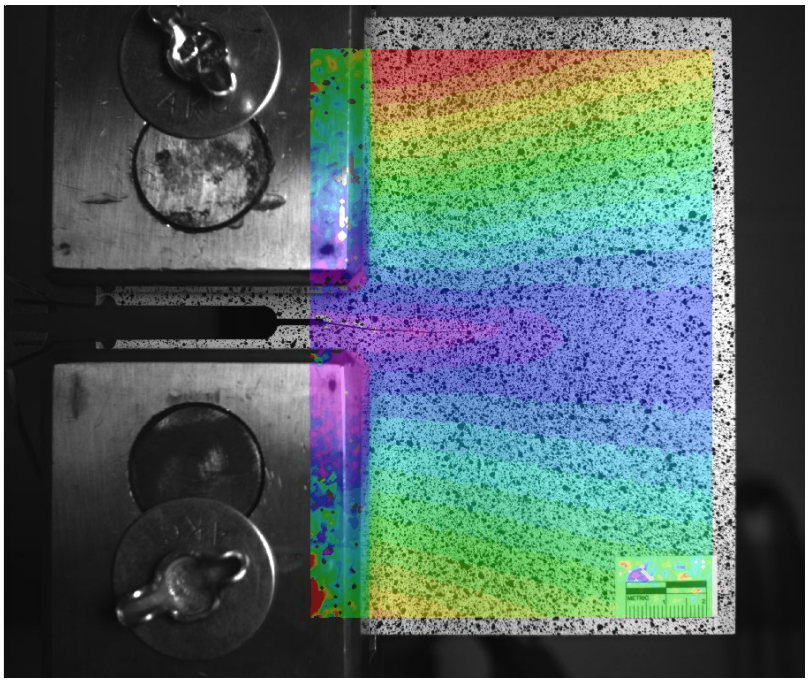

Figure A.54 Displacement contours for C(T) specimen with 38.1 mm (1.5 in.) in-plane crack under loading case 5

Figure A.55 Unloaded C(T) specimen with 50.8 mm (2.0 in.) in-plane crack

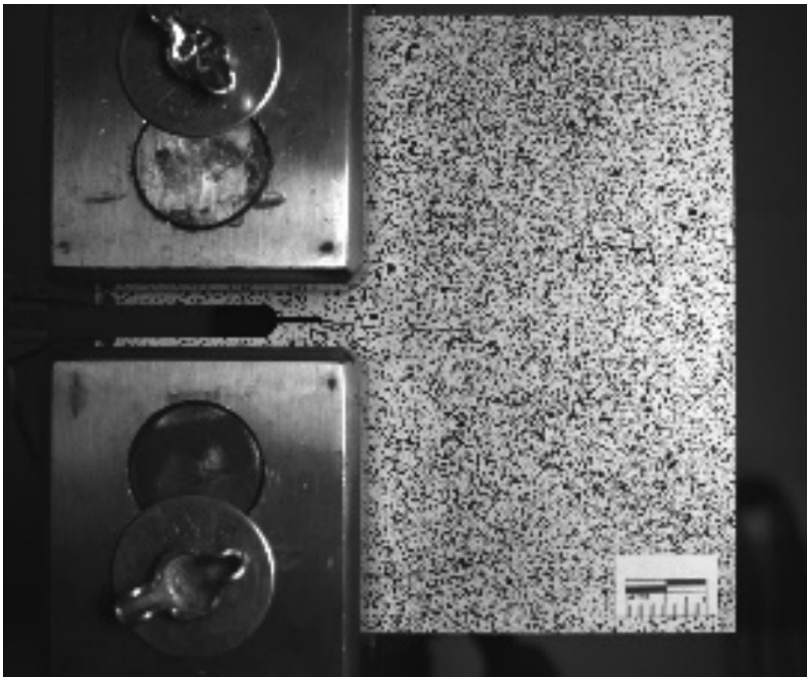

Figure A.56 C(T) specimen with 50.8 mm (2.0 in.) in-plane crack under loading case 1

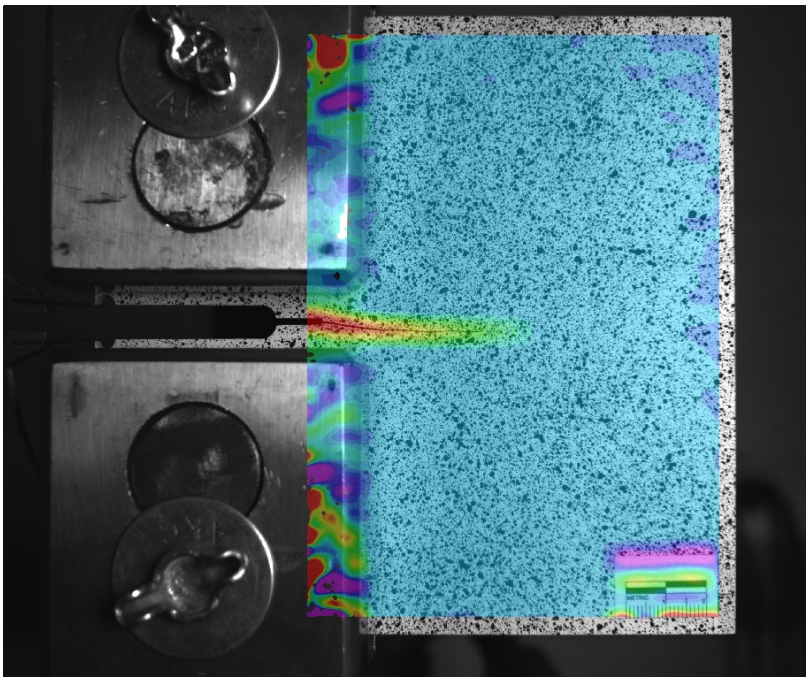

Figure A.57 Strain contours for C(T) specimen with 50.8 mm (2.0 in.) in-plane crack under loading case 1

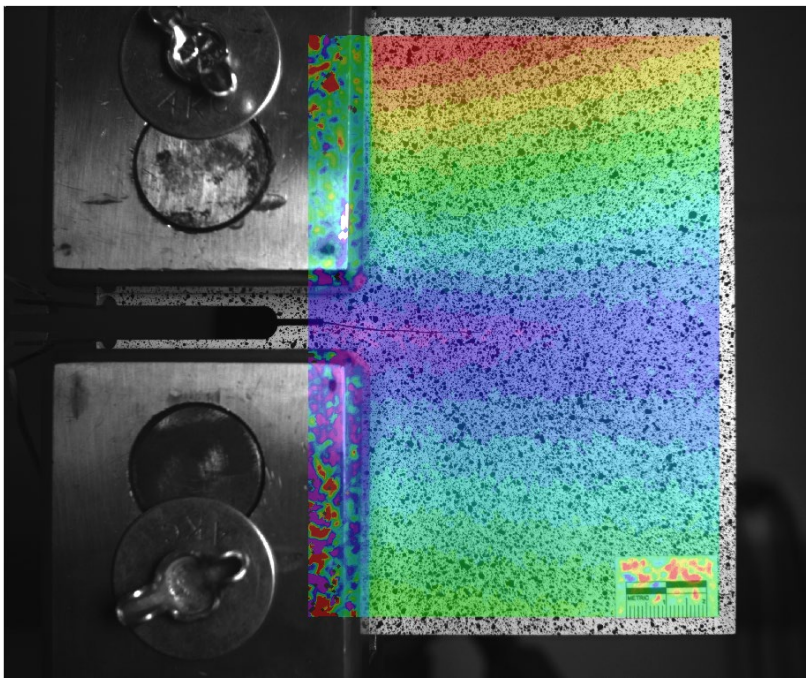

Figure A.58 Displacement contours for C(T) specimen with 50.8 mm (2.0 in.) in-plane crack under loading case 1

Figure A.59 C(T) specimen with 50.8 mm (2.0 in.) in-plane crack under loading case 2

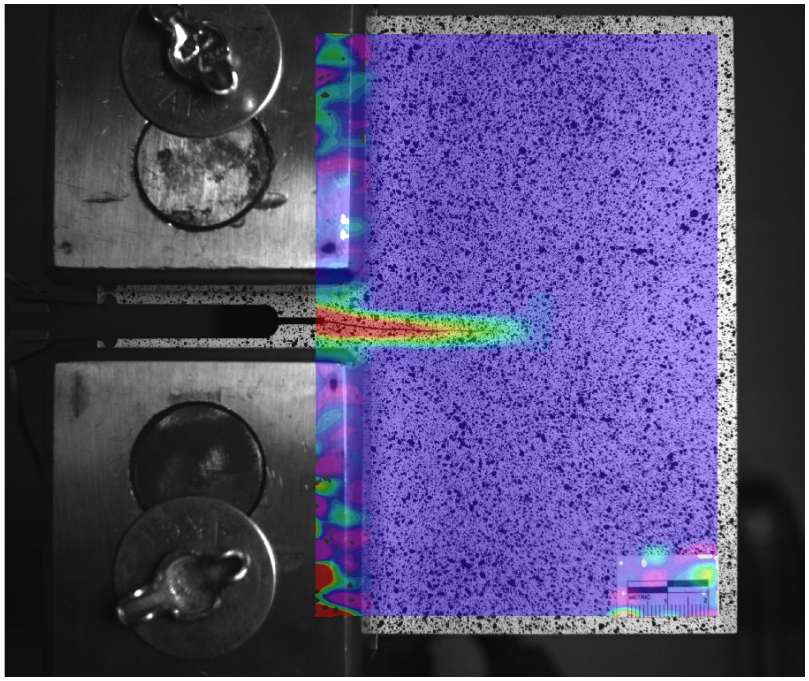

Figure A.60 Strain contours for C(T) specimen with 50.8 mm (2.0 in.) in-plane crack under loading case 2

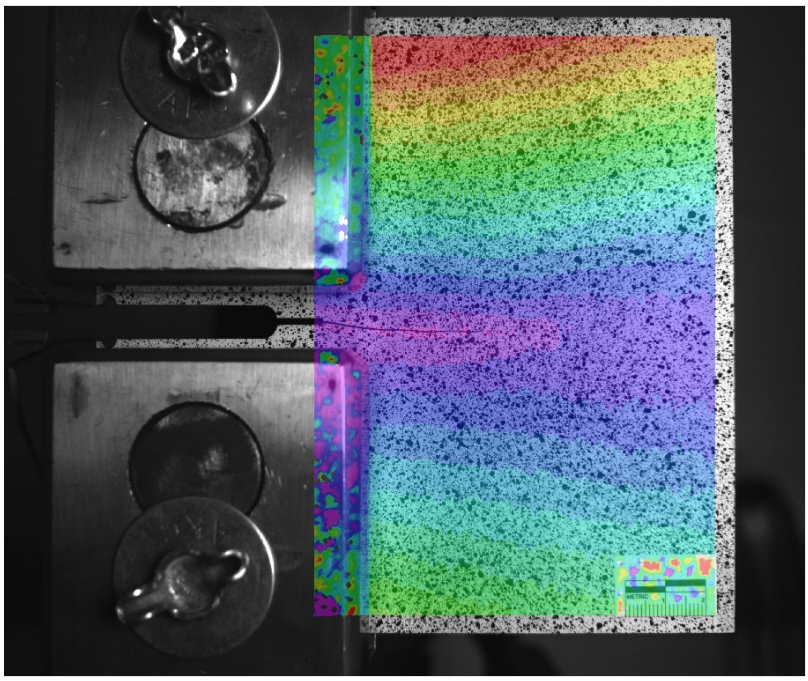

Figure A.61 Displacement contours for C(T) specimen with 50.8 mm (2.0 in.) in-plane crack under loading case 2

Figure A.62 C(T) specimen with 50.8 mm (2.0 in.) in-plane crack under loading case 3

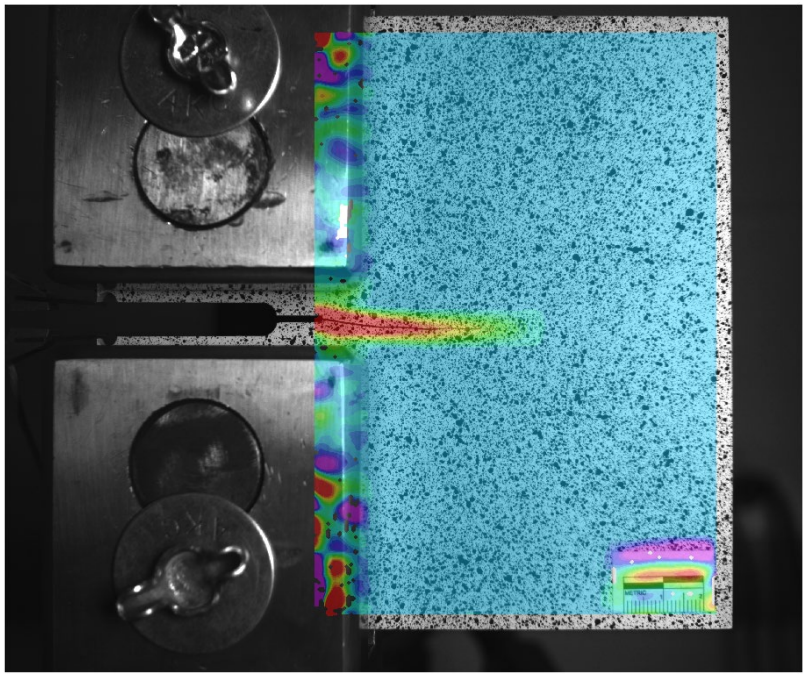

Figure A.63 Strain contours for C(T) specimen with 50.8 mm (2.0 in.) in-plane crack under loading case 3

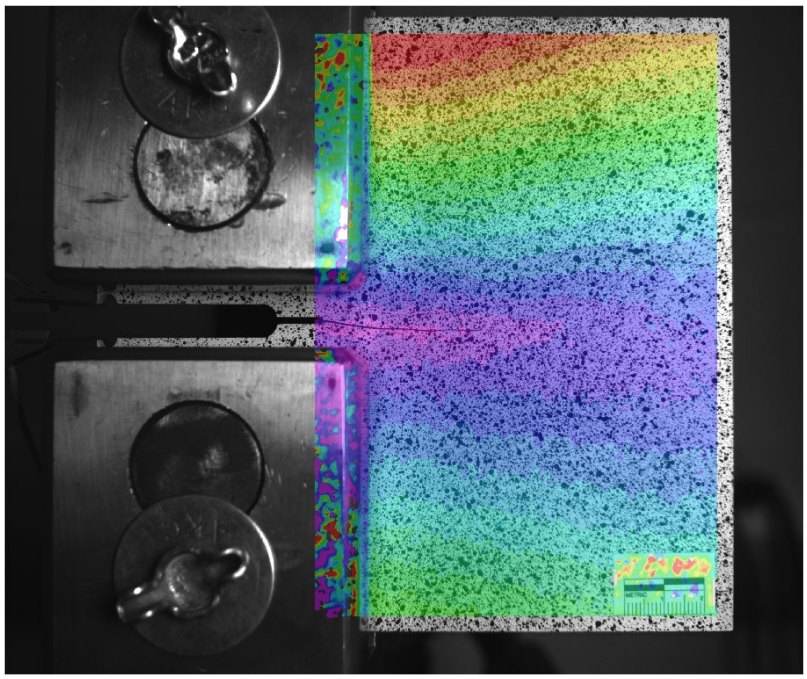

Figure A.64 Displacement contours for C(T) specimen with 50.8 mm (2.0 in.) in-plane crack under loading case 3

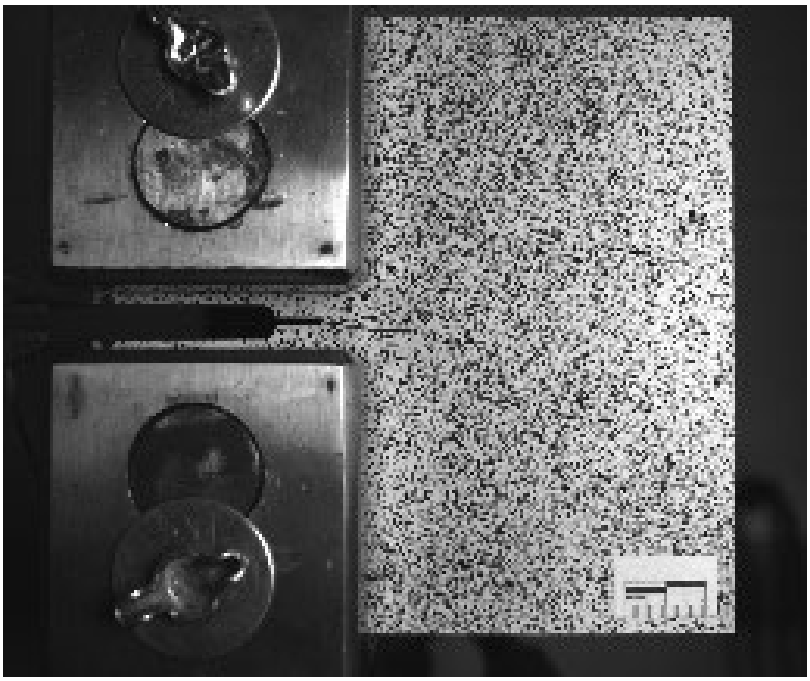

Figure A.65 C(T) specimen with 50.8 mm (2.0 in.) in-plane crack under loading case 4

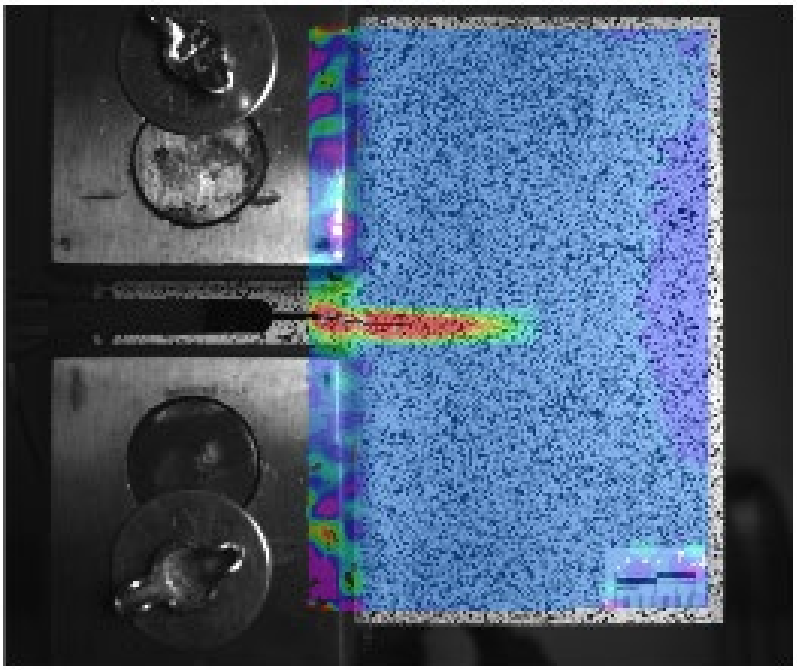

Figure A.66 Strain contours for C(T) specimen with 50.8 mm (2.0 in.) in-plane crack under loading case 4

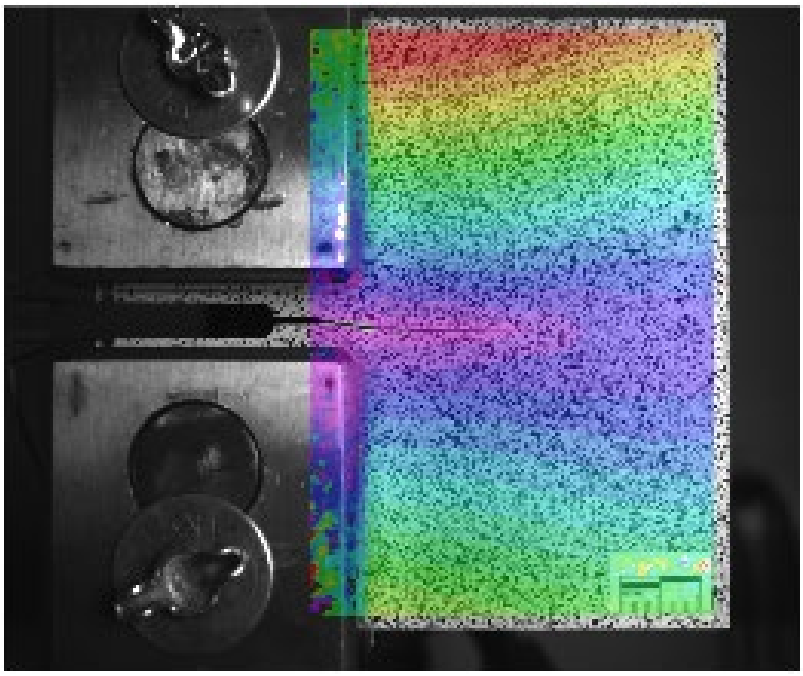

Figure A.67 Displacement contours for C(T) specimen with 50.8 mm (2.0 in.) in-plane crack under loading case 4

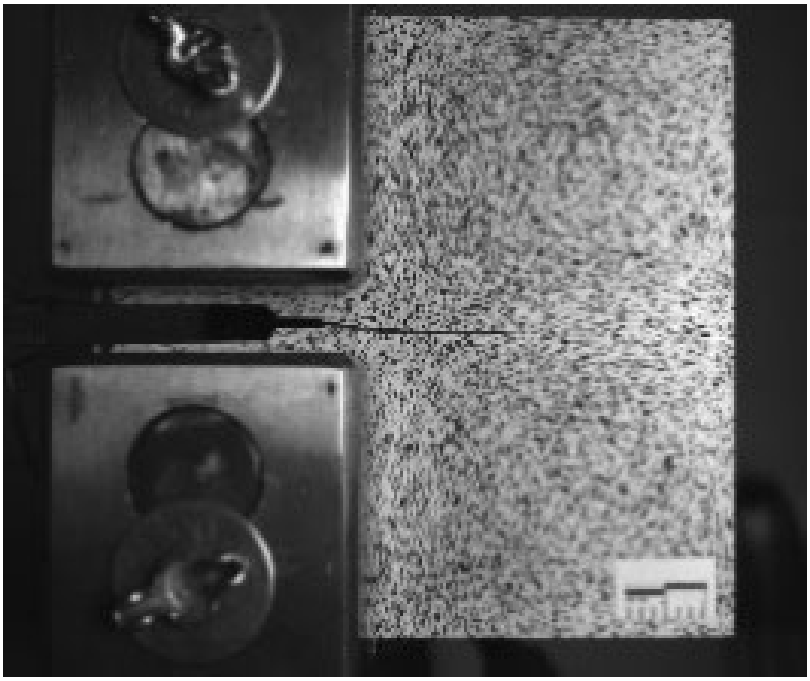

Figure A.68 C(T) specimen with 50.8 mm (2.0 in.) in-plane crack under loading case 5

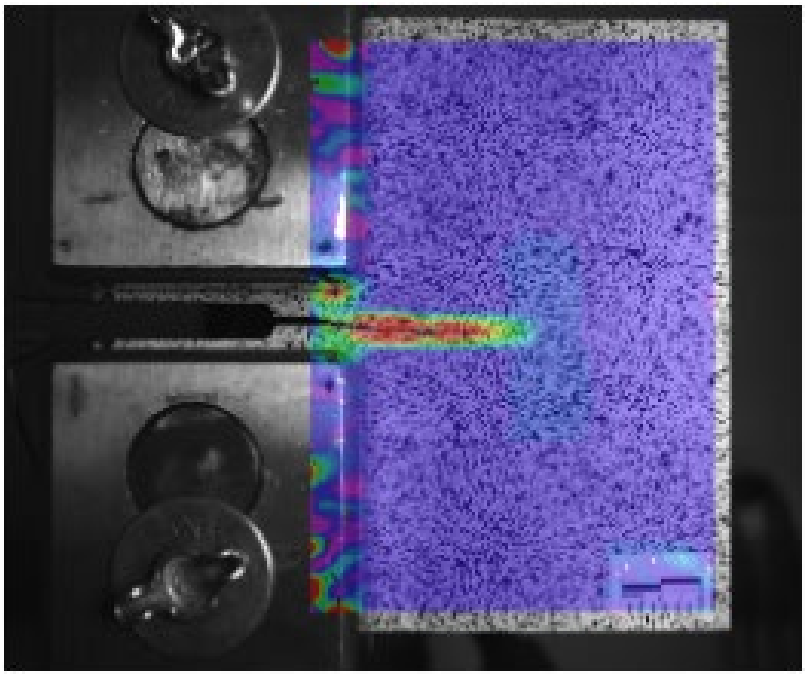

Figure A.69 Strain contours for C(T) specimen with 50.8 mm (2.0 in.) in-plane crack under loading case 5

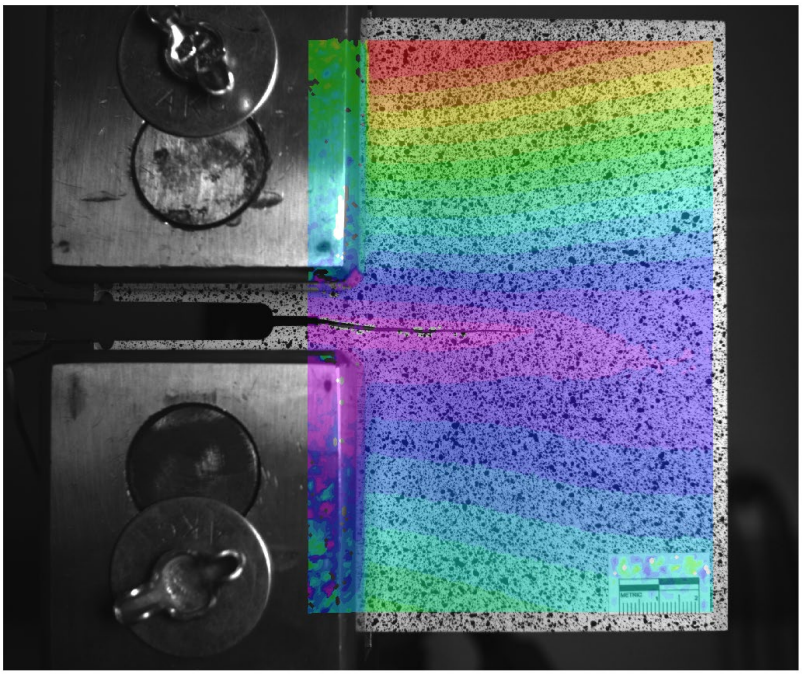

Figure A.70 Displacement contours for C(T) specimen with 50.8 mm (2.0 in.) in-plane crack under loading case 5

Appendix B Out-of-Plane Testing Data

Shown below are the strain and displacement contours for the out-of-plane testing.

Figure B.1 Unloaded out-of-plane specimen with 44.5 mm (1.75 in.) crack

Figure B.2 Out-of-plane specimen under loading case 1

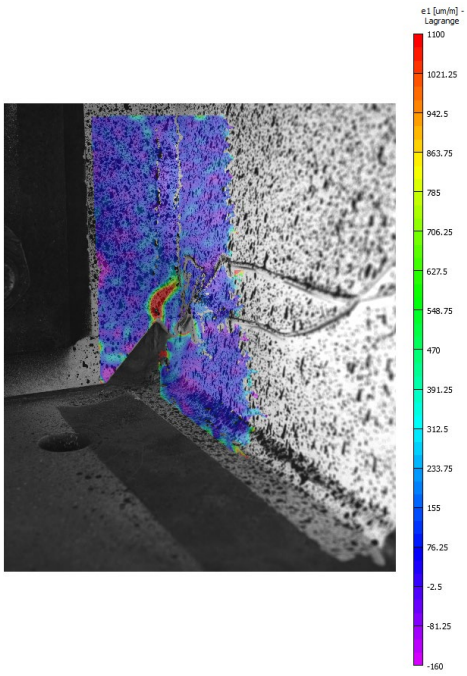

Figure B.3 Strain contours for out-of-plane specimen under loading case 1

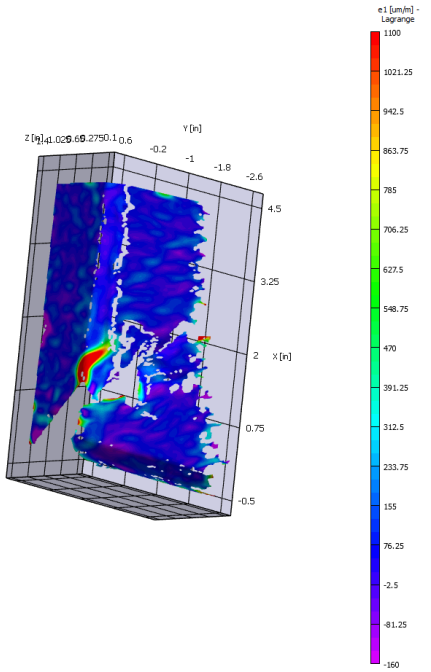

Figure B.4 3D graph of strain contours for out-of-plane specimen under loading case 1

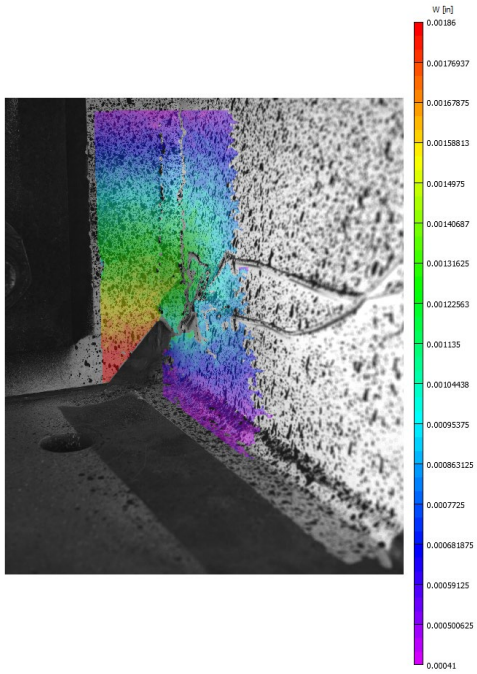

Figure B.5 Displacement contours for out-of-plane specimen under loading case 1

Figure B.6 Out-of-plane specimen under loading case 2

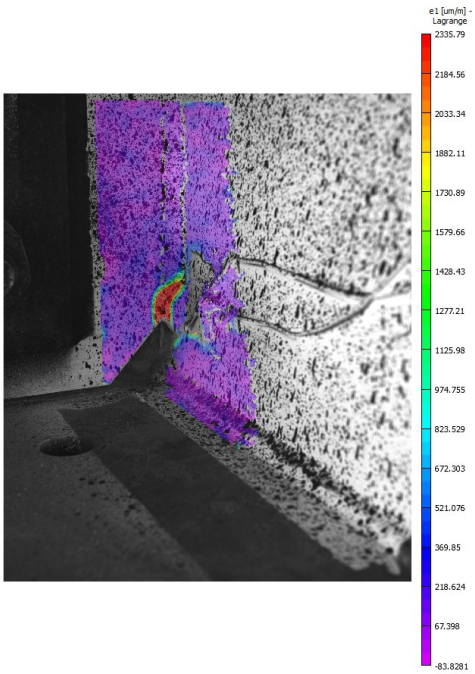

Figure B.7 Strain contours for out-of-plane specimen under loading case 2

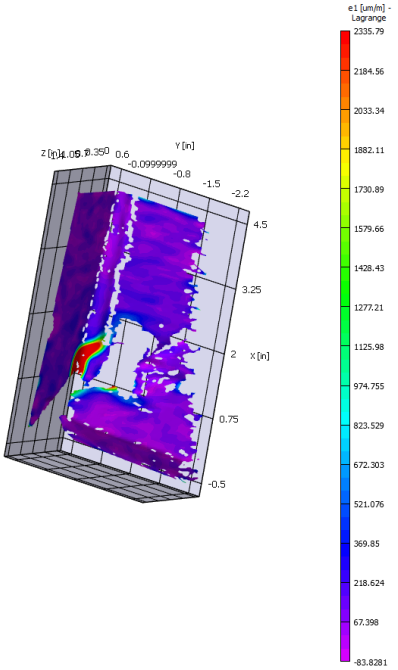

Figure B.8 3D graph of strain contours for out-of-plane specimen under loading case 2

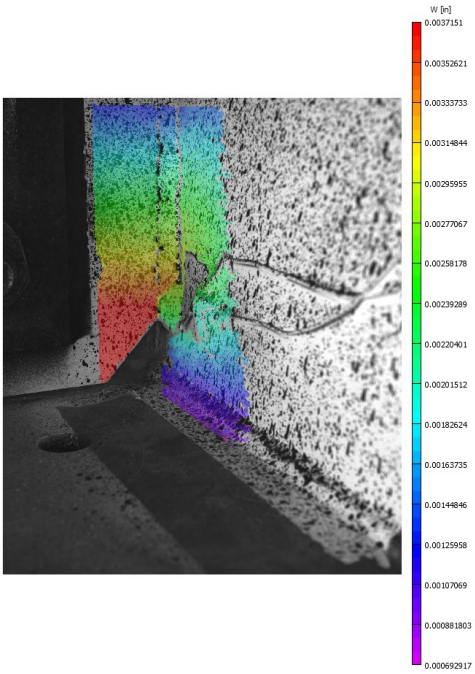

Figure B.9 Displacement contours for out-of-plane specimen under loading case 2

Figure B.10 Out-of-plane specimen under loading case 3

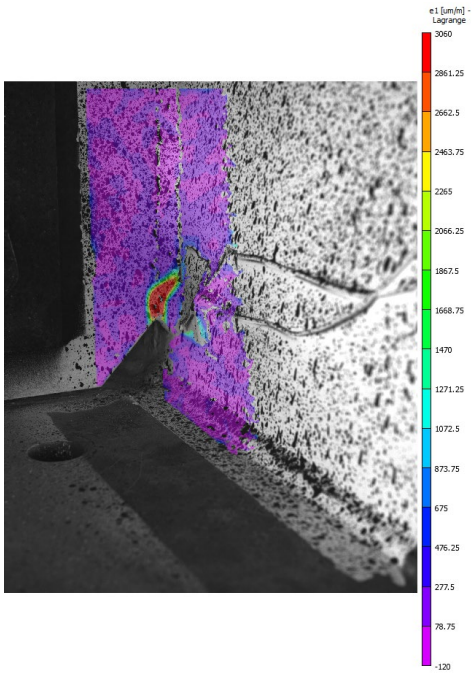

Figure B.11 Strain contours for out-of-plane specimen under loading case 3

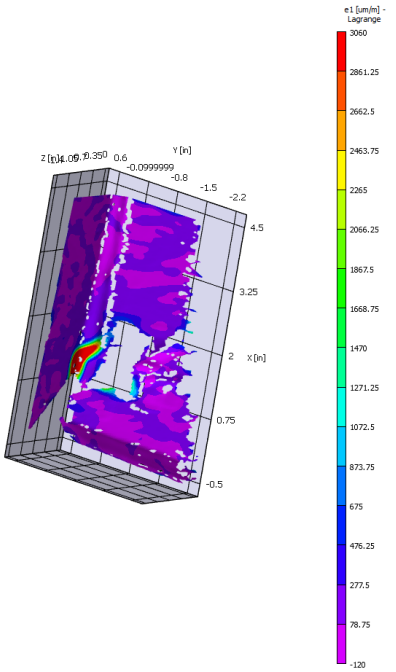

Figure B.12 3D graph of strain contours for out-of-plane specimen under loading case 3

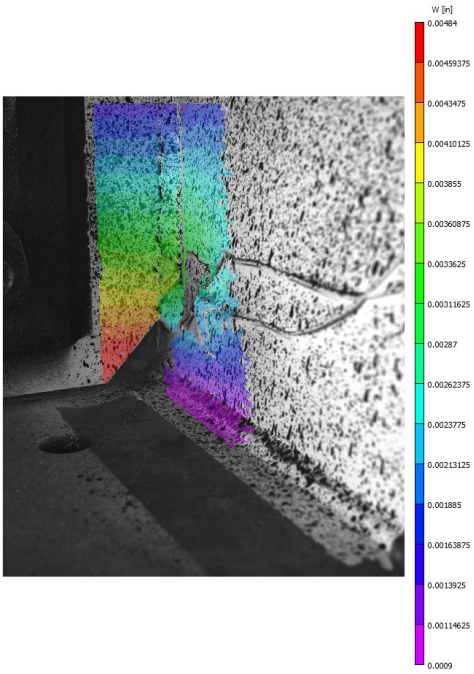

Figure B.13 Displacement contours for out-of-plane specimen under loading case 3

Figure B.14 Out-of-plane specimen under loading case 4

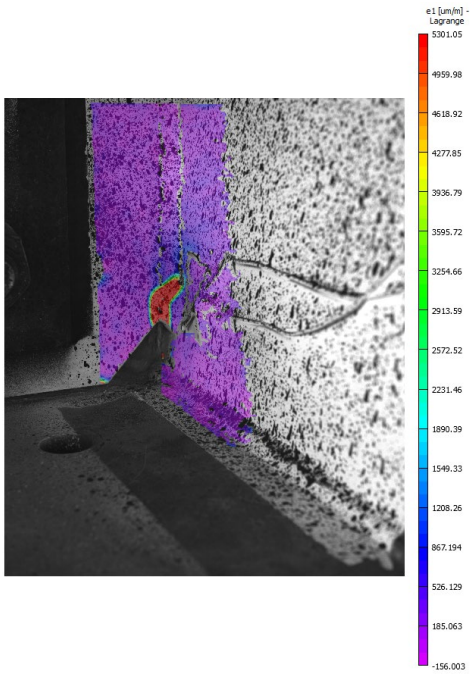

Figure B.15 Strain contours for out-of-plane specimen under loading case 4

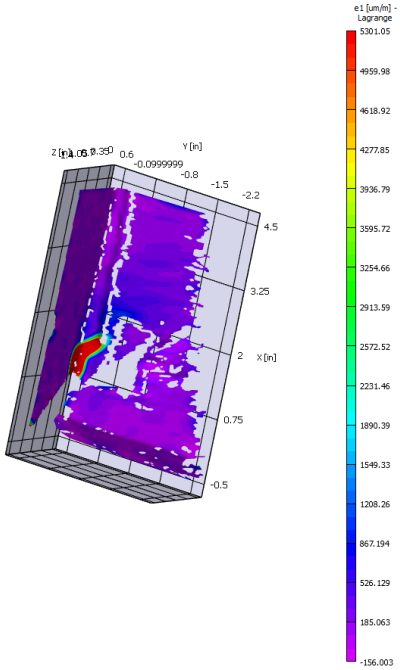

Figure B.16 3D graph of strain contours for out-of-plane specimen under loading case 4

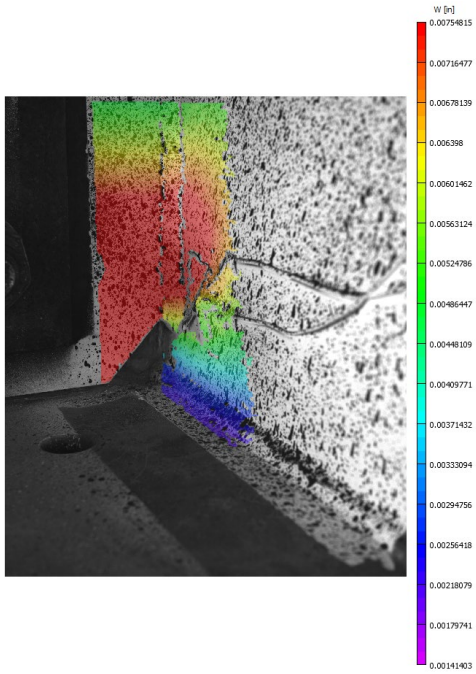

Figure B.17 Displacement contours for out-of-plane specimen under loading case 4

Figure B.18 Out-of-plane specimen under loading case 5

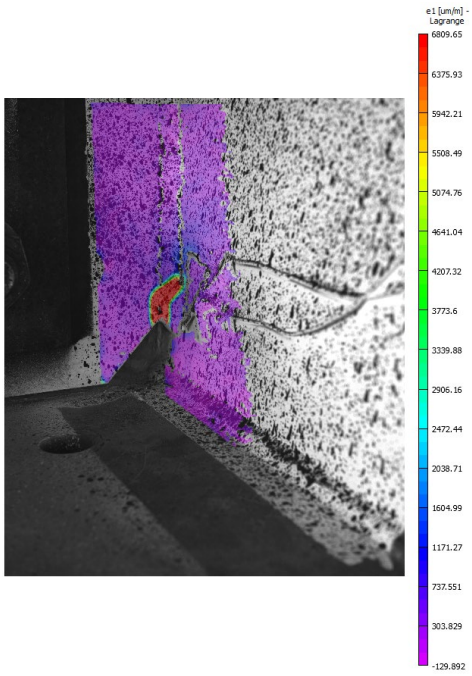

Figure B.19 Strain contours for out-of-plane specimen under loading case 5

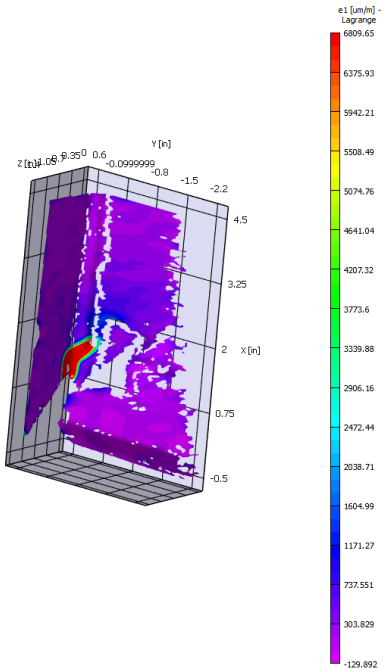

Figure B.20 3D graph of strain contours for out-of-plane specimen under loading case 5

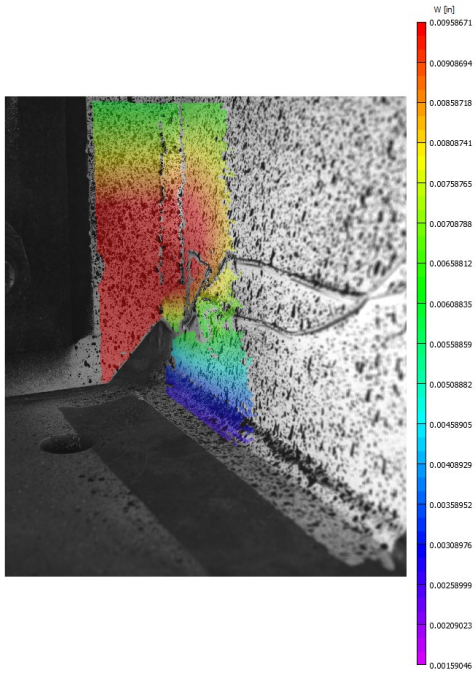

Figure B.21 Displacement contours for out-of-plane specimen under loading case 5

Figure B.22 Out-of-plane specimen under loading case 6

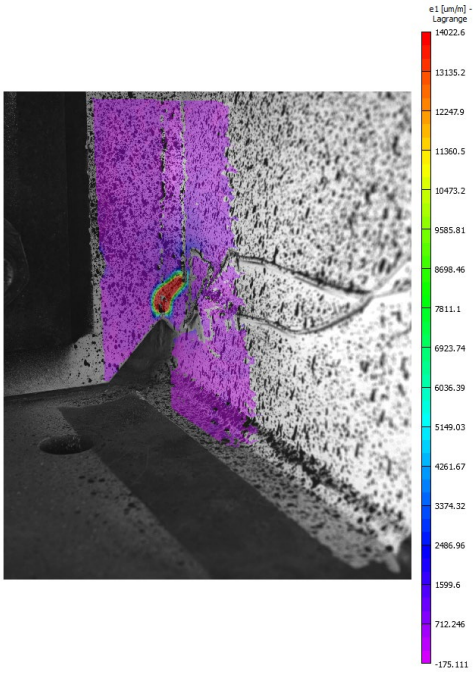

Figure B.23 Strain contours for out-of-plane specimen under loading case 6

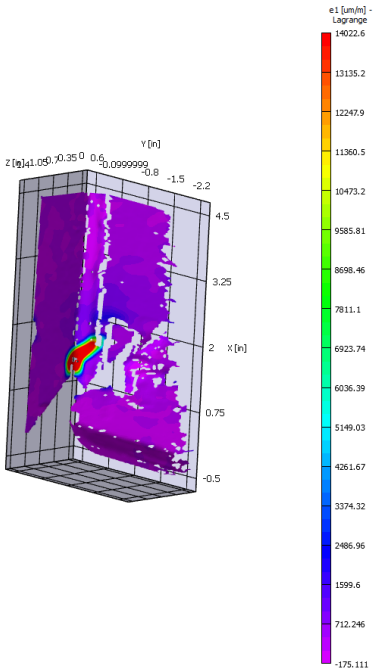

Figure B.24 3D graph of strain contours for out-of-plane specimen under loading case 6

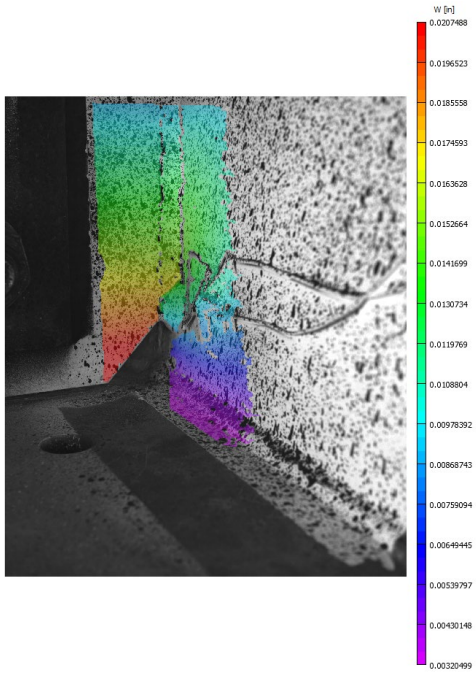

Figure B.25 Displacement contours for out-of-plane specimen under loading case 6

Figure B.26 Out-of-plane specimen under loading case 7

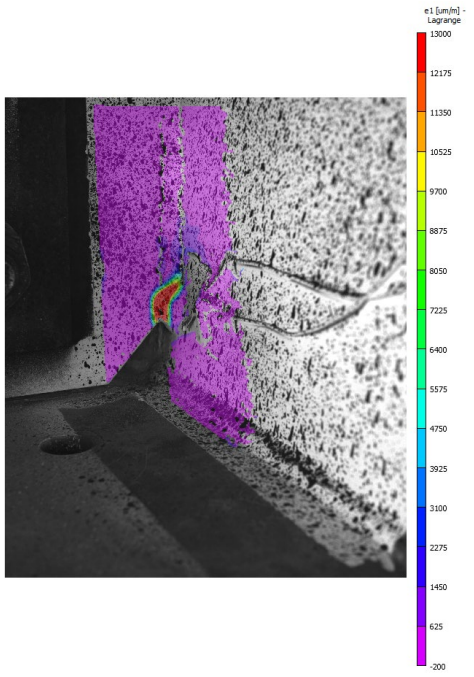

Figure B.27 Strain contours for out-of-plane specimen under loading case 7

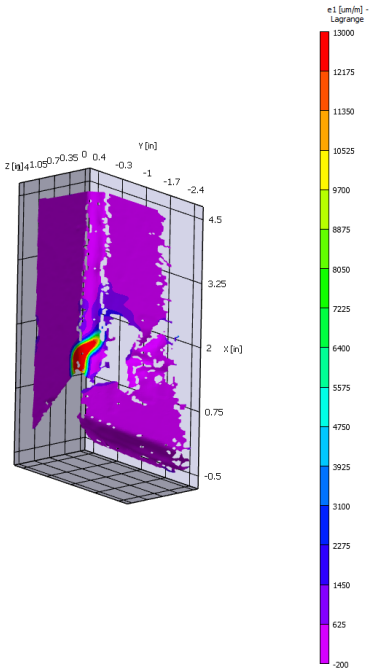

Figure B.28 3D graph of strain contours for out-of-plane specimen under loading case 7

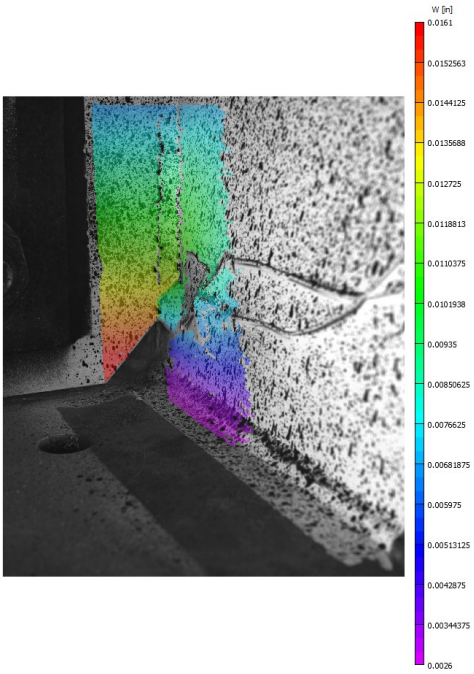

Figure B.29 Displacement contours for out-of-plane specimen under loading case 7